



Search for resonant $t\bar{t}$ production in proton-proton collisions at $\sqrt{s} = 8$ TeV

The CMS Collaboration*

Abstract

A search is performed for the production of heavy resonances decaying into top-antitop quark pairs in proton-proton collisions at $\sqrt{s} = 8$ TeV. Data used for the analyses were collected with the CMS detector and correspond to an integrated luminosity of 19.7 fb^{-1} . The search is performed using events with three different final states, defined by the number of leptons (electrons and muons) from the $t\bar{t} \rightarrow WbWb$ decay. The analyses are optimized for reconstruction of top quarks with high Lorentz boosts, where jet substructure techniques are used to enhance the sensitivity. Results are presented for all channels and a combination is performed. No significant excess of events relative to the expected yield from standard model processes is observed. Upper limits on the production cross section of heavy resonances decaying to $t\bar{t}$ are calculated. A narrow leptophobic topcolor Z' resonance with a mass below 2.4 TeV is excluded at 95% confidence level. Limits are also derived for a broad Z' resonance with a 10% width relative to the resonance mass, and a Kaluza–Klein excitation of the gluon in the Randall–Sundrum model. These are the most stringent limits to date on heavy resonances decaying into top-antitop quark pairs.

Published in Physical Review D as doi:10.1103/PhysRevD.93.012001.

1 Introduction

The top quark is the heaviest known fundamental particle, with a mass close to the electroweak scale. It has a Yukawa coupling to the Higgs potential close to unity, and is, therefore, closely connected to the hierarchy problem, where the largest corrections to the mass of the Higgs boson arise from top-quark loops. Studies of top-quark production may provide further insight into the mechanism of electroweak symmetry breaking, especially in the light of the recent discovery of a Higgs boson [1–3] and a precision measurement of its mass [4–6].

Many theories beyond the standard model (SM) predict the existence of heavy resonances, generically referred to as Z' , that preferentially decay to $t\bar{t}$ pairs and manifest themselves as a resonant component on top of the SM $t\bar{t}$ continuum production. Examples of such models include colorons [7–9] including a leptophobic topcolor Z' [10], extended gauge theories with massive color-singlet Z' bosons [11–13], axigluons [14, 15], and models in which a pseudoscalar Higgs boson may couple strongly to top quarks [16]. Furthermore, various extensions of the Randall–Sundrum model [17] with extra dimensions predict Kaluza–Klein (KK) excitations of gluons g_{KK} [18] or gravitons G_{KK} [19], both of which can have enhanced couplings to $t\bar{t}$ pairs.

Direct searches for heavy $t\bar{t}$ resonances have been performed at the Fermilab Tevatron and the CERN LHC colliders, with no evidence for such signals. The experiments at the Tevatron have probed the mass range up to about 900 GeV [20–25], using the leptophobic Z' model, and the LHC experiments have set subpicobarn limits on the production cross section in the mass range of 1–3 TeV [26–31].

This paper presents a model-independent search for $Z' \rightarrow t\bar{t} \rightarrow W^+bW^-\bar{b}$ production, where the leptonic and hadronic decay modes of the W bosons are considered. Unless otherwise indicated, the symbol Z' is used in the following to refer to the resonance decaying to $t\bar{t}$, irrespective of the specific model. This results in final states with two, one, or zero leptons, which are referred to as the dilepton, lepton+jets, and all-hadronic channels, respectively. The search is based on pp collision data collected by the CMS experiment at the LHC at a center-of-mass energy $\sqrt{s} = 8$ TeV, and corresponding to an integrated luminosity of 19.7 fb^{-1} .

The final state of the dilepton channel consists of two leptons of opposite charge (ee , $e\mu$, or $\mu\mu$) with high transverse momentum (p_{T}), at least two jets from the fragmentation of b quarks, and missing transverse momentum due to escaping neutrinos. The final-state objects arising from decays of heavy $t\bar{t}$ resonances are collimated because of the large Lorentz boosts of the top quark decay products. Leptons from the W boson decay are reconstructed in the proximity of jets from the fragmentation of b quarks. Special selection criteria are used to preserve high lepton selection efficiency for non-isolated leptons at high resonance masses. The dominant irreducible background is the $t\bar{t}$ continuum production. Other SM processes contributing to the background are single top quarks, Z +jets, and diboson production.

The final state considered in the lepton+jets channel consists of one high- p_{T} lepton (e or μ), at least two jets, of which at least one jet is identified to arise from the fragmentation of a b quark, and missing transverse momentum. As in the case of the dilepton analysis, special selection criteria are used to identify non-isolated leptons at high resonance masses. A top-quark tagging algorithm, referred to as a t tagging algorithm, is applied to identify fully hadronic decays of the type $t \rightarrow Wb \rightarrow q\bar{q}'b$ merged into one single jet. The use of the t tagging algorithm enhances the sensitivity of this channel at high resonance masses by about 30%–40%, and leaves $t\bar{t}$ continuum production as the dominant irreducible background. A bottom-quark tagging algorithm is also used to create regions enhanced in signal for the analysis.

The all-hadronic channel considers events with a dijet topology, where two wide jets are se-

lected and required to be consistent with the decay of a top quark. Two separate regions are explored: a search region sensitive to Z' masses $M_{Z'}$ below 1 TeV, where Cambridge-Aachen (CA) jets [32, 33] with a distance parameter of $R = 1.5$ are considered, and a search region for high resonance masses, using CA jets with $R = 0.8$. Two distinct t tagging algorithms [34, 35] are used for these two regions. In both regions the dominant background from non-top quark multijet production can be reduced considerably by requiring one identified subjet in each of the two top quark candidates to be consistent with the fragmentation of a b or c quark, leaving irreducible SM $t\bar{t}$ continuum production as the dominant background.

Except for the non-top multijet backgrounds in the all-hadronic channels, the shapes of all SM backgrounds are estimated from simulation. The total yield of the simulated samples is obtained with a binned maximum likelihood fit to the reconstructed $t\bar{t}$ invariant mass ($M_{t\bar{t}}$) distributions. A limit on the production cross section of heavy resonances is extracted by performing a template-based statistical evaluation of the $M_{t\bar{t}}$ distributions of all channels.

This paper is organized as follows: Section 2 gives a description of the CMS detector. The reconstruction and identification of electrons, muons, and jets is described in Section 3. Section 3 also gives an overview of the t tagging algorithms used. The data sets and simulated Monte Carlo (MC) samples used in the analysis are given in Section 4. Section 5 describes the event selection for the three different channels. Systematic uncertainties are discussed in Section 6, while Section 7 describes the evaluation of the SM background processes. The statistical analysis and the results are given in Section 8, and a summary is given in Section 9.

2 CMS detector

The central feature of the CMS detector is a superconducting solenoid of 6 m internal diameter, providing a magnetic field of 3.8 T. Within the solenoid volume are a silicon pixel and strip tracker, a lead tungstate crystal electromagnetic calorimeter, and a brass and scintillator hadron calorimeter, each composed of a barrel and two endcap sections. In addition to the barrel and endcap detectors, CMS has extensive forward calorimetry. Muons are detected by four layers of gas-ionization detectors embedded in the steel flux-return yoke of the magnet. The inner tracker measures charged particle trajectories within the pseudorapidity range $|\eta| < 2.5$, and provides an impact parameter resolution of approximately $15 \mu\text{m}$. A two-stage trigger system selects pp collision events of interest for use in physics analyses. A more detailed description of the CMS detector, together with a definition of the coordinate system used and the relevant kinematic variables, can be found in Ref. [36].

3 Event reconstruction

The CMS experiment uses a particle-flow (PF) based event reconstruction [37, 38], which aggregates input from all subdetectors. This information includes charged-particle tracks from the tracking system and deposited energy from the electromagnetic and hadronic calorimeters, taking advantage of excellent granularity of the sub-systems. Particles are classified as electrons, muons, photons, charged hadrons, and neutral hadrons. Primary vertices are reconstructed using a deterministic annealing filter algorithm [39]. The vertex with the largest squared sum of the associated track p_T values is taken to be the primary event vertex.

Electrons are reconstructed in the pseudorapidity range $|\eta| < 2.5$, by combining tracking information with energy deposits in the electromagnetic calorimeter [40, 41]. Electron candidates are required to originate from the primary event vertex. Electrons are identified using infor-

mation on the shower shape, the track quality, and the spatial match between the track and electromagnetic cluster, and the fraction of total cluster energy in the hadron calorimeter. Electron candidates that are consistent with originating from photon conversions in the detector material are rejected.

Muons are detected and measured in the pseudorapidity range $|\eta| < 2.4$ using the information collected in the muon and tracker detectors [42]. Tracks from muon candidates must be consistent with a muon originating from the primary event vertex and satisfy track fit quality requirements.

Since the top-quark decay products can be collimated at high values of $M_{Z'}$, no isolation requirements on the leptons are imposed in either the trigger or offline selections.

The missing transverse momentum vector \vec{p}_T^{miss} is defined as the projection on the plane perpendicular to the beams of the negative vector sum of the momenta of all reconstructed particles in an event. Its magnitude is referred to as E_T^{miss} .

Particle-flow candidates are clustered into jets using the FASTJET 3.0 software package [43]. Charged hadrons associated with other event vertices than the primary event vertex are removed prior to jet clustering. All jets are required to satisfy $|\eta| < 2.4$. The dilepton and lepton+jets analyses use jets obtained by the anti- k_T jet-clustering algorithm [44] with a distance parameter of 0.5 (AK5 jets). If a lepton candidate (electron or muon) is found within $\Delta R < 0.5$ of an AK5 jet, its four-momentum is subtracted from that of the jet. In this paper the unmodified term ‘jet’ will refer to these AK5 jets. The all-hadronic analyses use the CA jet-clustering algorithm [32, 33] with distance parameters of 0.8 (CA8 jets) and 1.5 (CA15 jets) for the analyses at high and low values of the $t\bar{t}$ invariant mass, respectively. The CA algorithm has been chosen because of its use in the declustering of jets for the identification of jet substructure. The CA8 jets are also employed in the lepton+jets analysis to identify the hadronic decay of top quarks with high p_T in the hemisphere opposite to one defined by the momentum vector of the lepton. All jets contain neutral particles from additional collisions in the beam crossing (pileup). The extra contribution is subtracted based on the average expectation of the pileup in the jet catchment area [45]. This is done by calculating a correction for the average offset energy density in each event as function of the number of primary vertices [46]. Jets are identified as originating from the fragmentation of a b or c quark by the combined secondary vertex algorithm (CSV). The loose and medium operating points are used, which were chosen to have a misidentification probability of 10% and 1%, respectively, for tagging light-parton jets with an average p_T of about 80 GeV. The efficiency for the medium operating point varies between 70%–75% for jet p_T in the range 50–100 GeV, where it reaches a plateau. Above 200 GeV the efficiency decreases gradually to about 60% for p_T values of 500 GeV [47]. All jets are required to satisfy quality selections to remove calorimeter noise and other sources of fake jets [48]. Events are required to also satisfy selection criteria to remove calorimeter noise from E_T^{miss} signals as described in Ref. [49].

The structure of CA jets is used to distinguish hadronically decaying top quarks merged into a single jet from light quark or gluon jets. For CA8 jets the CMS t tagging algorithm is used [50, 51], which is based on an algorithm studied in Ref. [34]. Only jets with $p_T > 400$ GeV are considered, as at lower momenta the decay products of the hadronically decaying top quark are rarely merged into a single jet. The algorithm attempts to split the merged jets into subjets. In the process, soft and wide-angle particles relative to the parent in the clustering are ignored, enhancing the separation into subjets. CA8 jets that pass the CMS t tagging algorithm (CA8 t-tagged jets) are required to have at least three subjets. The mass of the jet has to satisfy the condition $140 < M_{\text{jet}} < 250$ GeV, the minimum pairwise mass M_{min} of the three highest p_T

subjects is required to be greater than 50 GeV, and the N -subjettiness [52, 53] ratio $\tau_{32} \equiv \tau_3/\tau_2$ must be smaller than the value of 0.7, which has been obtained from optimization studies. The N -subjettiness observable τ_N , defined through the relation

$$\tau_N = \frac{1}{d_0} \sum_i p_{T,i} \min[\Delta R_{1,i}, \Delta R_{2,i}, \dots, \Delta R_{N,i}],$$

is a measure of the consistency of a CA jet with N or fewer subjects, where i is a sum over all jet constituents, and the ΔR terms represent distances between a given constituent i and one of the N candidate subjet axes. The quantity d_0 is a normalization constant.

The HEPTopTagger [35] algorithm is applied to CA15 jets. The larger distance parameter allows the identification of hadronic decays of top quarks with intermediate transverse momenta, $p_T > 200$ GeV. The CA15 jet is decomposed according to the last clustering step of the CA algorithm. Subjects are identified by an iterative procedure: when undoing the last clustering of the jet into two subjects, the mass of the heavier subjet is required to be between 30 GeV and 80% of the mass of the original jet. The algorithm fails if fewer than three subjects are found. If three or more subjects are reconstructed, jet constituents are reclustered using the CA algorithm with filtering [54] until there are exactly three subjects. Additional criteria are applied to the invariant mass calculated from the three subjects and the pairwise masses using combinations of the three subjects to reject jets from light quarks or gluons [51]. Jets identified by the HEPTOPTAGGER are referred to as CA15 t-tagged jets [55].

In the all-hadronic channel, additional discriminating power against background processes is obtained from the application of the CSV algorithm to the subjects of the CA jets. A CA jet is considered to be b-tagged if the subjet with the highest discriminator value satisfies the requirement for the medium operating point. This has an efficiency of about 65% and a misidentification probability of approximately 5%. In the following, this algorithm will be called subjet b tagging. Its performance has been studied in data, and shows a gain in efficiency for boosted topologies with respect to the standard b tagging algorithm [56]. The same study also compared the b-quark efficiency in data and simulated events, and established that the measured data-to-simulation scale factor for b-tagged subjects is the same as for unmerged b jets.

4 Trigger and data sets

Dilepton events are collected with single-lepton triggers. Events for the ee channel are selected using a single electron trigger with a p_T threshold of 80 GeV and an efficiency of 90%. In all cases, no isolation requirement is applied to the leptons. Similarly, $e\mu$ and $\mu\mu$ events are recorded with a trigger requiring a single muon with $p_T > 40$ GeV and $|\eta| < 2.1$. The efficiency for this trigger is 95% for muons measured within $|\eta| < 0.9$, 85% if they are measured within $0.9 < |\eta| < 1.2$ and 83% for $1.2 < |\eta| < 2.1$.

The data used in the lepton+jets channel also rely on single lepton triggers. The trigger for electron events requires one electron with $p_T > 35$ GeV in conjunction with two jets that have $p_T > 100$ and 25 GeV, respectively. The trigger for muon events is the same one used in the dilepton analysis. In both cases, no isolation requirement is applied to the leptons. A 10% increase in the signal efficiency at $M_{Z'} = 2$ TeV is gained in the electron channel by including events that are triggered by a single jet with $p_T > 320$ GeV. The events recovered by the single-jet trigger contain an electron merged in a jet, which can not be resolved at the trigger level. The resulting trigger efficiency is 90% for events with a leading (highest p_T) jet with $p_T < 320$ GeV. Above this value the trigger shows a turn-on behavior and is fully efficient above a value of 350 GeV.

The all-hadronic data sample is based on two different triggers. The first requires the scalar sum of the p_T of jets (H_T) to be greater than 750 GeV, with an efficiency of 95% or higher after the analysis selection. The second requires four jets with $p_T > 50$ GeV at trigger level, used to gain efficiency in the low mass regime with $M_{Z'} < 1$ TeV. The efficiency of this trigger is 50% for events with the fourth leading jet having $p_T > 50$ GeV, and increases to 100% for jets with $p_T > 100$ GeV.

The total integrated luminosity associated with the datasets is 19.7 fb^{-1} , except for the four-jet data set, which corresponds to an integrated luminosity of 18.3 fb^{-1} . The lower integrated luminosity in the latter case is due to the unavailability of the four-jet trigger at the start of data taking. The efficiencies for all triggers are well modeled by the simulation.

The $Z' \rightarrow t\bar{t}$ process is simulated using the MADGRAPH 4.4 [57] event generator, which produces a generic high-mass resonance with the same left- and right-handed couplings to fermions as the SM Z boson. Higher-order parton radiations are calculated for up to three extra partons at tree level. The simulation is performed for masses $M_{Z'}$ of 0.75, 1, 1.25, 1.5, 2, and 3 TeV, and for relative decay widths $\Gamma_{Z'}/M_{Z'}$ of 1% (narrow-width) and 10% (wide-width). Kaluza–Klein gluon excitations are simulated using PYTHIA 8 [58], where interference effects with SM $t\bar{t}$ production are neglected. The widths of the g_{KK} signals are about 15%–20% of the resonance mass. For visualization purposes, the signal samples are scaled to an arbitrary cross section of 1 pb. This is about a factor of 30 larger than the cross section expected from the narrow-width topcolor Z' model.

Figure 1 shows the invariant mass of the $t\bar{t}$ quark system at the parton level for the Z' and g_{KK} samples for two different invariant masses, 1.5 and 3 TeV. The samples at 1.5 TeV show a peaked structure, characteristic of a narrow-width resonance. The samples at 3 TeV exhibit a significant tail at low invariant mass values due to the interplay between the available partonic center-of-mass energy and the width of the resonance; this is most pronounced for g_{KK} because of its very large width. Above 3 TeV, the resonant hypothesis for the signal samples is not valid anymore, thus signals with masses above 3 TeV are not considered in this paper.

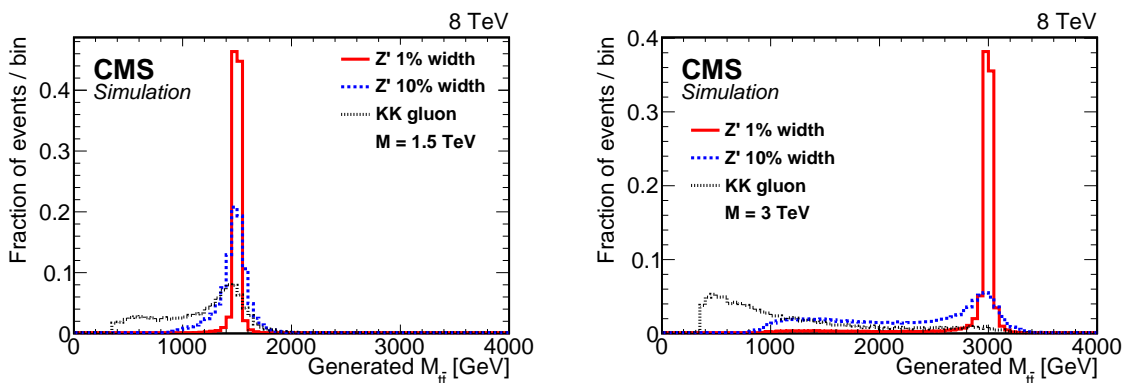


Figure 1: The invariant mass distributions for different signal models, as described in the text, for (left) 1.5 TeV and (right) 3 TeV masses.

Top-quark events, produced via the strong and electroweak interactions, are simulated using the next-to-leading-order (NLO) generator POWHEG 1.0 [59–61]. The $W(\rightarrow l\nu)+\text{jets}$ and $Z/\gamma^*(\rightarrow ll)+\text{jets}$ processes are simulated using MADGRAPH 5.1 [62], and the diboson production processes (WW , WZ , and ZZ) are simulated using PYTHIA 6.424 [63]. Simulated QCD multijet samples produced with MADGRAPH are used to validate the estimation of the multijet background from data.

All of the samples produced with MADGRAPH are interfaced to PYTHIA for parton showering and fragmentation. The MLM algorithm [64] is applied during the parton matching to avoid double counting of partons. The MADGRAPH samples use the CTEQ6L [65] parton distribution functions (PDF). For the POWHEG $t\bar{t}$ sample, the CT10 [66] PDF set is utilized, whereas the single top quark processes are produced with the CTEQ6M PDF set. The most recent PYTHIA 6 Z2* tune is used to model the underlying event activity. It is derived from the Z1 tune [67], which uses the CTEQ5L parton distribution set, whereas Z2* uses CTEQ6L [68].

The leading-order (LO) cross sections for the topcolor Z' signal are taken from Ref. [10], whereas for g_{KK} production, calculations from Ref. [18] are used. However, both cross sections are multiplied by a factor of 1.3 to approximate NLO effects [69]. The normalizations of the background samples are taken from the NLO+next-to-next-to-leading logarithms (NNLL) calculation for the single top quark production [70], the next-to-next-to-leading order (NNLO) calculations for $W(\rightarrow \ell\nu)+\text{jets}$ and $Z/\gamma^*(\rightarrow \ell\ell)+\text{jets}$ [71–73], and the NLO calculation for diboson production [74]. The normalization for the continuum $t\bar{t}$ background uses NNLO calculations [75]. However, by comparing the number of simulated and data events in control regions, we determine additional cross section scale factors. This is discussed in Section 5.

A detailed simulation of particle propagation through the CMS apparatus and detector response is performed with GEANT4 v9.2 [76]. For all simulated samples, the hard interaction collision is overlaid with a number of simulated minimum bias collisions. The resulting events are weighted to reproduce the pileup distribution measured in data. The same event reconstruction software is used for data and simulated events. The resolutions and efficiencies for reconstructed objects are corrected to match those measured in data [40, 42, 47, 49, 51].

5 Reconstruction of $t\bar{t}$ events

5.1 Dilepton channel

In the dilepton channel, the selection is based on the assumption that both W bosons decay leptonically. The selection requires two leptons and at least two jets. The lepton and the b quark from the decay of a highly Lorentz-boosted top quark are usually not well separated, resulting in a non-isolated lepton that partially or fully overlaps with the b -quark jet.

Offline, the following selection requirements are applied. In the ee channel, events are required to have two electrons with $p_T > 85$ GeV and $p_T > 20$ GeV, each within $|\eta| < 2.5$. In the $e\mu$ channel, there must be a muon with $p_T > 45$ GeV with $|\eta| < 2.1$ and an electron with $p_T > 20$ GeV with $|\eta| < 2.5$. Events in the $\mu\mu$ channel should contain two muons with $p_T > 45$ GeV and $p_T > 20$ GeV with $|\eta| < 2.1$ and $|\eta| < 2.4$, respectively. In all three channels, the two lepton candidates must have opposite charge. The invariant mass of the lepton candidates in the ee and $\mu\mu$ channels must be $M_{\ell\ell} > 12$ GeV and outside the mass window of $76 < M_{\ell\ell} < 106$ GeV. These selections reduce the contribution from the production of low-mass resonances and from on-shell Z boson production. Events are required to contain at least two jets with $p_T > 100$ GeV and $p_T > 50$ GeV within $|\eta| < 2.5$.

Signal events are selected with a two-dimensional isolation variable that is efficient at high top-quark boosts yet reduces multijet backgrounds. This two-dimensional isolation requires $\Delta R(\ell, \text{jet}) > 0.5$ or $p_{T,\text{rel}}(\ell, \text{jet}) > 15$ GeV, where $\Delta R(\ell, \text{jet})$ is the distance in (η, ϕ) between the lepton and the nearest jet, and $p_{T,\text{rel}}(\ell, \text{jet})$ is the transverse momentum of the lepton with respect to the axis of the closest jet. In calculating these quantities only jets with $p_T > 30$ GeV are considered. The efficiency of the two-dimensional isolation requirement has been studied in

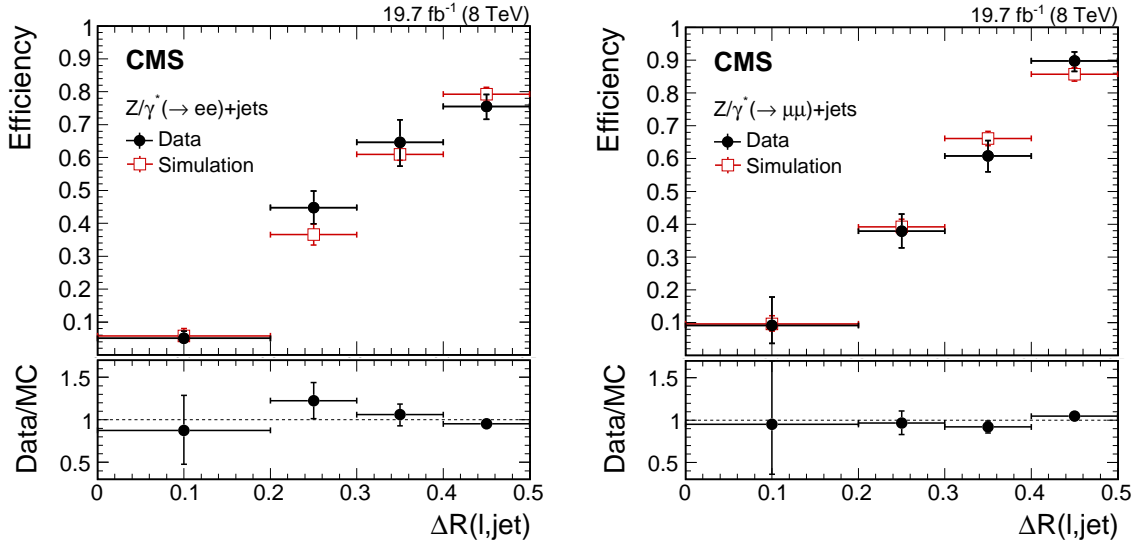


Figure 2: Efficiency of the two-dimensional isolation requirement for data and simulated events for the electron (left) and muon (right) selection, as measured in a sample of $Z/\gamma^*(\rightarrow \ell\ell)+\text{jets}$. The ratio of the efficiencies in data to simulation is shown at the bottom of each panel.

data and simulation in a $Z/\gamma^*(\rightarrow \ell\ell)+\text{jets}$ sample. In this sample, one lepton, passing isolation criteria, is used as a tag, and the other lepton is used as a probe to study the efficiency. The dilepton invariant mass is used to determine the number of events passing and failing the two-dimensional isolation criteria. Figure 2 shows the efficiency as function of $\Delta R(\ell, \text{jet})$ for data and simulated events. At small ΔR separation between the lepton and the closest jet, the efficiency for electrons is 5%, increasing to 75% for larger $\Delta R(\ell, \text{jet})$. The corresponding values are 10% to 90% for muons. The efficiency is well described by the simulation and no correction is needed. The relative efficiency of the two-dimensional isolation requirement for the 1.5 TeV signal is approximately 70% independent of width.

A requirement of $E_{\text{T}}^{\text{miss}} > 30 \text{ GeV}$ in the ee and $\mu\mu$ channels additionally reduces the contribution from multijet and $Z/\gamma^*(\rightarrow \ell\ell)+\text{jets}$ production. Given the presence of two b quarks in the events, a logical OR of two b tagging algorithms is used: at least one of the two leading jets is required to be tagged as a b-quark jet by the CSV algorithm at the medium working point or both leading jets must be tagged using the loose working point of the CSV algorithm. After these requirements, the sample contains about 90% $t\bar{t}$ background.

The boosted nature of the signal events provides an additional handle for further reduction of the $t\bar{t}$ background: the separation in ΔR between each lepton and its nearest jet. Requiring $\Delta R(\ell_1, \text{jet}) < 1.2$ and $\Delta R(\ell_2, \text{jet}) < 1.5$, where ℓ_1 and ℓ_2 denote the leading and sub-leading leptons, reduces the $t\bar{t}$ background contribution by more than a factor of 2, while the loss for a Z' signal with mass of 1.5 TeV is about 10%. Additionally, the region with $\Delta R(\ell_2, \text{jet}) > 1.5$ is dominated by events from continuum $t\bar{t}$ production and provides an independent sample to check the $t\bar{t}$ background normalization. The contamination from resonant $t\bar{t}$ production is expected to be less than 0.2% in this sample. The normalization of the $t\bar{t}$ background is found to be compatible with the SM expectation using the NNLO cross section calculations, and good agreement between the ee , $e\mu$, and $\mu\mu$ channels is observed.

The resonant nature of the signal is exploited by constructing a mass variable from the four-momenta of the two leading leptons, the two leading jets, and the neutrinos, which approximates the invariant mass of the $t\bar{t}$ system. For the momentum components p_x and p_y of the pair of neutrinos, the x - and y -components of $\vec{p}_{\text{T}}^{\text{miss}}$ are used, and the p_z component of each neutrino

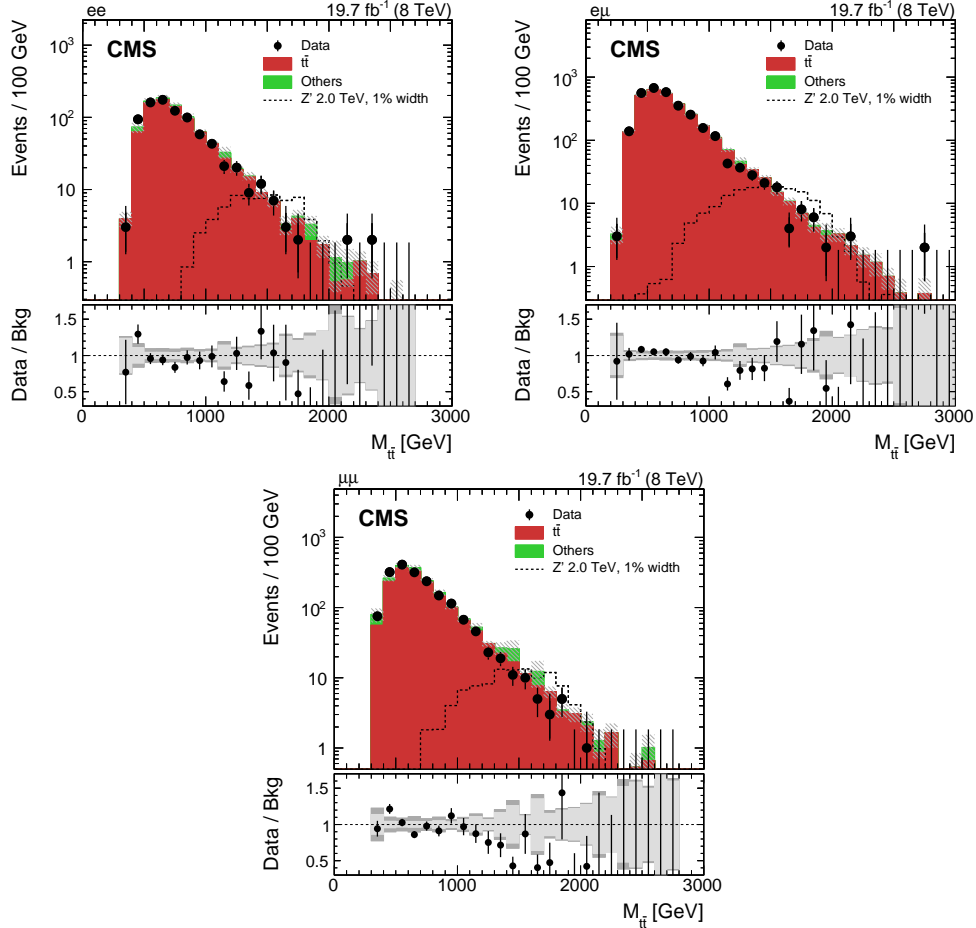


Figure 3: Reconstructed invariant mass of the $t\bar{t}$ pair in the ee (upper left), $e\mu$ (upper right), and $\mu\mu$ (bottom) channels for data and simulated events. Each background process is scaled by a factor derived from a maximum likelihood fit to data. The expected distribution from a Z' signal with $M_{Z'} = 2$ TeV and $\Gamma_{Z'}/M_{Z'} = 0.01$, normalized to a cross section of 1 pb, is also shown. The uncertainty associated with the background expectation includes all the statistical and systematic uncertainties. For bins with no events in data but with nonzero background expectation, vertical lines are shown indicating the 68% confidence level coverage corresponding to an observation of zero events. The data-to-background ratio is shown in the bottom panel of each figure. For the ratio plot, the statistical uncertainty is shown in light gray, while the total uncertainty, which is the quadratic sum of the statistical and systematic uncertainties, is shown in dark gray. There is a systematic disagreement observed in the high-mass region that is accommodated by the renormalization and factorization scale uncertainty.

is set to zero.

Figure 3 shows the $M_{\bar{t}\bar{t}}$ distributions for the dilepton channel. The expected distribution from a Z' signal with $M_{Z'} = 2$ TeV is also shown. Good agreement between the data and the SM background expectation is found.

5.2 Lepton+jets channel

The selection in the lepton+jets channel is based on events with one W boson decaying leptonically, $W \rightarrow \ell\nu$, and the other one decaying hadronically, $W \rightarrow q\bar{q}'$. It requires one lepton (electron or muon) and at least two jets with high p_T , including events with non-isolated leptons and merged jets arising from decays of two high- p_T top quarks.

Events are required to have exactly one electron with $p_T > 35$ GeV and $|\eta| < 2.5$, or one muon with $p_T > 45$ GeV and $|\eta| < 2.1$. The reconstructed lepton has to be consistent with originating from the primary event vertex. In order to avoid overlap with the dilepton sample, events with a second reconstructed lepton are removed. All events must have at least two jets with $p_T > 150$ GeV and $p_T > 50$ GeV, both with $|\eta| < 2.4$. In order to ensure that there is no overlap with the all-hadronic channel, events with two or more CA8 t-tagged jets are rejected. To reduce the background from multijet production, events are required to have $E_T^{\text{miss}} > 50$ GeV and the scalar sum of the lepton p_T and E_T^{miss} has to be larger than 150 GeV.

A further reduction of the multijet background contribution is achieved by applying a similar two-dimensional isolation criterion as described for the dilepton channel. It is applied for both the electron and muon channels, requiring $\Delta R(\ell, \text{jet}) > 0.5$ or $p_{T,\text{rel}}(\ell, \text{jet}) > 25$ GeV, where only jets with $p_T > 25$ GeV are considered when calculating these quantities.

In addition, in the electron channel topological requirements are imposed that ensure that \vec{p}_T^{miss} does not point along the transverse direction of the electron or the leading jet [29],

$$|\Delta\phi(\{\text{e or jet}\}, \vec{p}_T^{\text{miss}}) - 1.5| < E_T^{\text{miss}}/50 \text{ GeV}$$

with E_T^{miss} measured in GeV. The efficiency of this requirement is above 95% for all signal samples, while the background from multijet production is reduced significantly.

The $\bar{t}\bar{t}$ system is reconstructed by assigning the four-vectors of the reconstructed final-state objects to either the leptonic or hadronic leg of the $\bar{t}\bar{t}$ decay. This is done by constructing a two-term χ^2 function, based on the masses of the reconstructed $\bar{t}\bar{t}$ candidates [29, 31]. For each event, the hypothesis with the smallest χ^2 value is chosen. In case a CA8 t-tagged jet is found in the event, this jet is used for the hadronic leg of the $\bar{t}\bar{t}$ decay and all jets with $\Delta R < 1.3$ from the t-tagged jet are removed from the list of possible hypotheses. Events are required to have a minimum value of χ^2 smaller than 50, which reduces the contribution from background processes and enhances the sensitivity of the search. In the electron channel, the transverse momentum of the reconstructed leptonic leg of the top-quark decay is required to be larger than 140 GeV, to suppress the background from multijet production to a negligible level.

Events are categorized based on the lepton flavor and on the number of CA8 t-tagged jets. In case no CA8 t-tagged jet is found, the events are further split into two categories, depending if any jets are identified as originating from the fragmentation of a b quark using the medium working point of the CSV algorithm. This has a tagging efficiency of 65% per jet [47].

An independent control sample is used to validate the mistag rate of CA8 t-tagged jets in the W+jets sample. This sample is obtained by inverting the χ^2 criterion, using the leptonic leg of the $\bar{t}\bar{t}$ decay hypothesis only, and requiring that no jet has been tagged as a b-quark jet by the

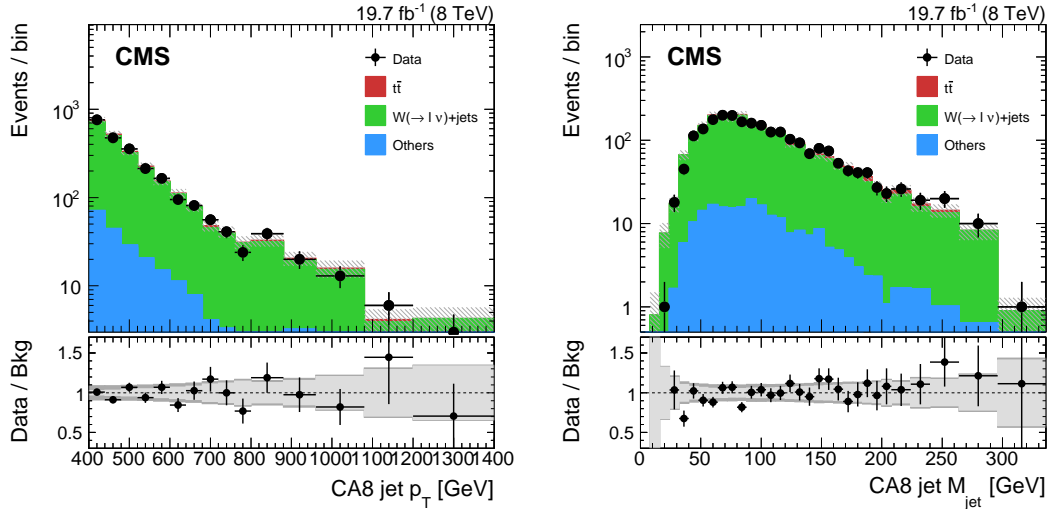


Figure 4: Distribution of p_T (left) and the jet mass (right) of the leading CA8 jet in a W+jets control region, used to obtain the mistag rate of CA8 t-tagged jets. The horizontal error bars indicate the bin width. The data-to-background ratio is shown in the bottom panel of each figure. For the ratio plot, the statistical uncertainty is shown in light gray, while the total uncertainty, which is the quadratic sum of the statistical and systematic uncertainties, is shown in dark gray.

loose operating point of the CSV algorithm [47]. This removes most of the $t\bar{t}$ contamination while retaining events from W+jets production. Figure 4 shows the p_T and mass of the leading CA8 jet in this sample. These jets are used to determine the mistag rate of the CA8 t-tagged jets in data and simulated events that also contain a lepton. Such events have a higher fraction of jets from quark fragmentation than the non-top-quark multijet background for the all-hadronic channel, which has a higher fraction of jets from gluon fragmentation. Good agreement is observed, with a mistag rate of 1.2% in data, and a data-to-simulation ratio of 0.83 ± 0.21 . This factor is used to scale simulated events containing a misidentified top-quark jet.

To validate the CA8 t tagging efficiency, distributions of the jet mass, minimum pairwise mass, and the ratio τ_{32} for CA8 t-tagged jets are shown in the lepton+jets channel for data and simulated events in Fig. 5, where all SM components are normalized to the output of the maximum likelihood fit. Differences between the distributions in data and simulation lead to different efficiencies of the t tagging algorithm. In order to account for these differences, a correction factor for simulated events is derived from a combined maximum likelihood fit. The fit is performed by comparing the yields in categories of events which pass and fail the CA8 t tagging selection criteria, as explained in Section 7. The scale factor for t-tagged jets is estimated to be 0.94 ± 0.03 , reflecting the somewhat better resolution of the reconstructed mass of CA8 jets in simulation.

The reconstructed top-quark candidates are used to calculate the $t\bar{t}$ invariant mass. The events are divided into six categories, three for each lepton+jets channel, so in total six $M_{t\bar{t}}$ distributions are obtained. The three categories for each lepton flavor are: events with one CA8 t-tagged jet, events without a CA8 t-tagged jet but at least one b tag, and events with neither a CA8 t-tagged jet nor a b tag. All six distributions are shown in Fig. 6.

5.3 All-hadronic channel

When the top quark has large p_T and decays hadronically, all decay products frequently merge into a single jet. Events with high $t\bar{t}$ invariant mass, where both quarks decay hadronically, thus

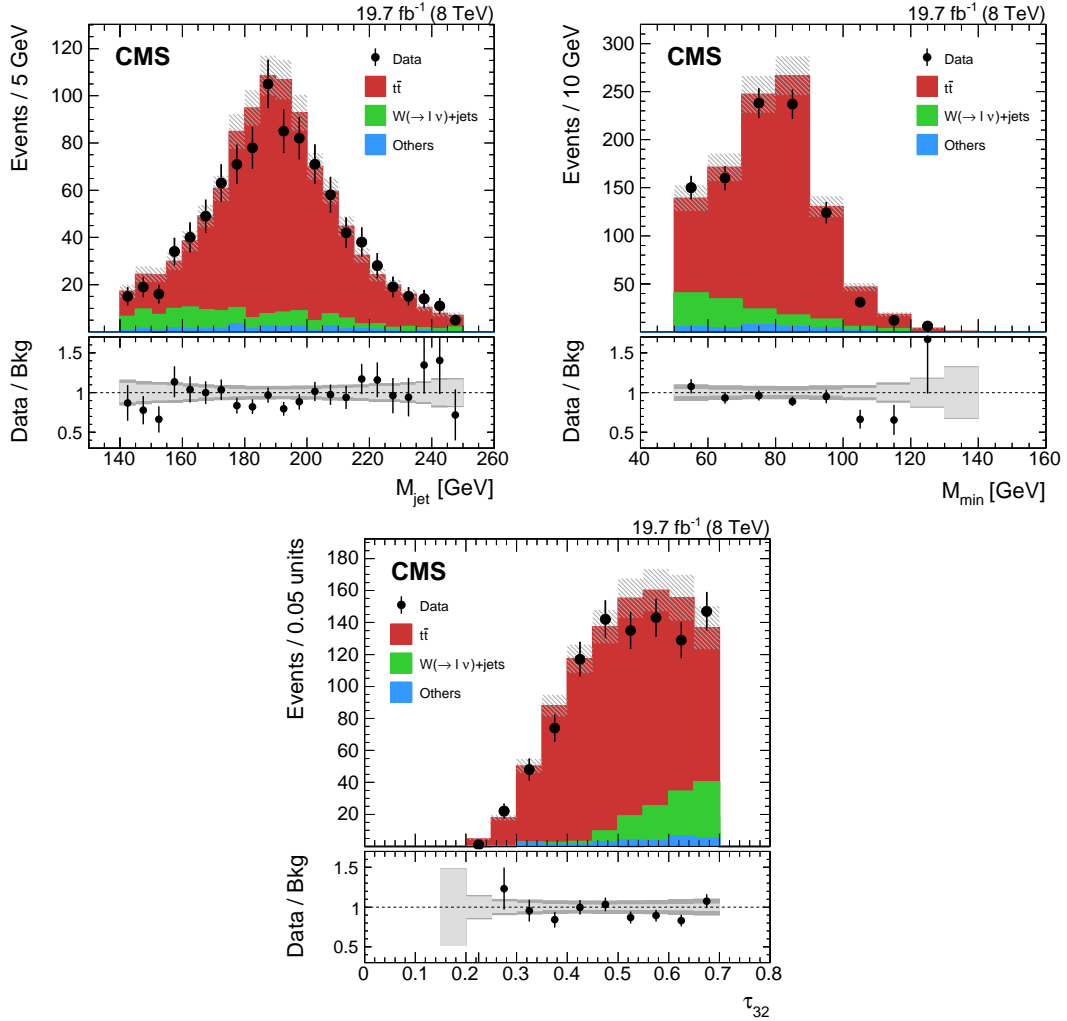


Figure 5: Distributions of the jet mass (upper left), minimum pairwise mass M_{\min} (upper right), and the ratio τ_{32} (bottom) for CA8 t -tagged jets in the lepton+jets channel. The SM backgrounds are scaled by a factor derived from the maximum likelihood fit to data. The uncertainty associated with the background expectation includes all the statistical and systematic uncertainties. The data-to-background ratio is shown in the bottom panel of each figure. For the ratio plot, the statistical uncertainty is shown in light gray, while the total uncertainty, which is the quadratic sum of the statistical and systematic uncertainties, is shown in dark gray.

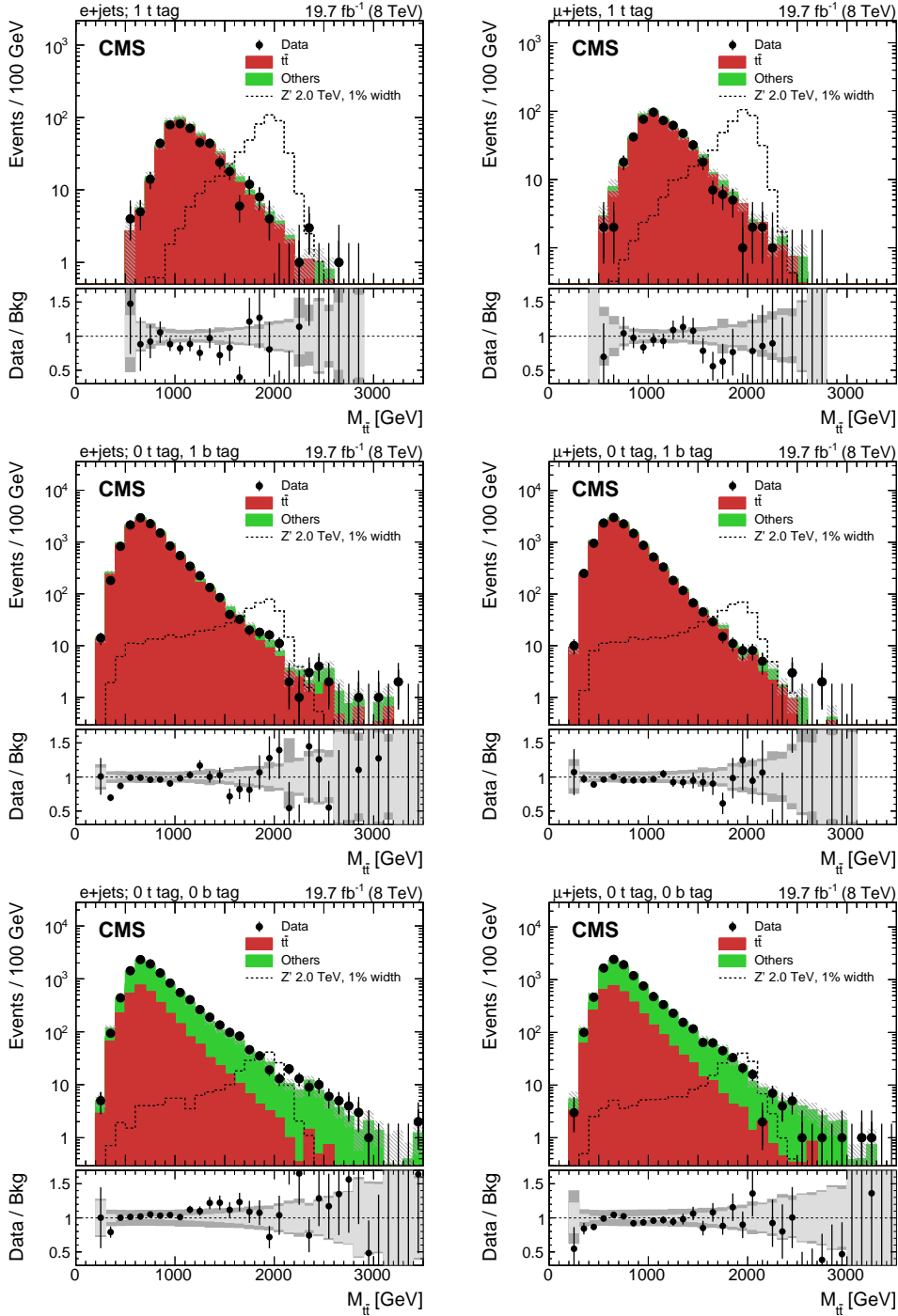


Figure 6: Invariant mass of the reconstructed $t\bar{t}$ pair in data and simulation in the electron+jets (left column) and muon+jets (right column) channels. Events are separated into three categories: one CA8 t -tagged jet (top row), no CA8 t -tagged jet and at least one b tag (middle row), and no CA8 t -tagged jet and no b tag (bottom row). Each background process is scaled by a factor derived from the maximum likelihood fit to data. The expected distribution from a Z' signal with $M_{Z'} = 2$ TeV and $\Gamma_{Z'}/M_{Z'} = 0.01$, normalized to a cross section of 1 pb, is also shown. The uncertainty associated with the background expectation includes all statistical and systematic uncertainties. For bins with no events in data but with non-zero background expectation, vertical lines are shown indicating the 68% confidence level coverage corresponding to an observation of zero events. The data-to-background ratio is shown in the bottom panel of each figure. For the ratio plot, the statistical uncertainty is shown in light gray, while the total uncertainty, which is the quadratic sum of the statistical and systematic uncertainties, is shown in dark gray.

effectively result in a dijet topology. This forms the basis of the selection in the all-hadronic channel. Two exclusive selections are made, one optimized for higher resonance masses, and one optimized for lower resonance masses where the decay products are still somewhat collimated.

To satisfy the high-mass selection, events are required to have two CA8 t-tagged jets with $p_T > 400$ GeV and rapidity $|y| < 2.4$. The two jets have to be separated in azimuthal angle by $|\Delta\phi| > 2.1$ radians. The rapidity difference between the two leading jets is also used to divide the events into two categories ($|\Delta y| < 1.0$ and $|\Delta y| > 1.0$), since the QCD multijet background with light-quark and gluon final states dominantly populates the $|\Delta y| > 1.0$ category, whereas the Z' signal with a mass of 2 TeV is equally split between the two. The two categories are further subdivided depending on the number of CA8 jets containing a b-tagged subjet: zero, one, or two. This results in six exclusive search regions, with the highest sensitivity in the categories with two b-tagged CA8 jets.

The low-mass selection is applied to events failing the high-mass selection and is designed to gain sensitivity in regions where the decay products are less collimated. Events are selected if two CA15 t-tagged jets with $p_T > 200$ GeV and $|y| < 2.4$ are found. The sample is split into events with $H_T < 800$ GeV and $H_T > 800$ GeV, where H_T is defined as the scalar sum of jet p_T , including all jets with $p_T > 50$ GeV. The sample is further categorized according to the number of b-tagged CA15 jets.

In order to estimate the background for the all-hadronic analysis, an approach based on control samples in data is applied. A sideband is selected by inverting the CA8 t tagging minimum mass requirement on one of the jets in the dijet sample. For the low-mass analysis, the CA15 t tagging selection criteria based on the subjet invariant mass and pairwise masses are inverted. The other leading CA jet in the event provides a kinematically unbiased ensemble of non-top-quark jets to measure the mistag rate. This mistag rate is then applied to the events where exactly one jet passes the t tagging selection. These events have a higher gluon fraction than the events used to derive the mistag rate for the lepton+jets analysis, as mentioned above.

The misidentification probability, r , for a non-t-quark CA jet to be identified as a t-tagged CA jet, is parametrized by three variables, the jet p_T , the N -subjettiness ratio τ_{32} , and the jet b tagging discriminant β (the output of the CSV algorithm described above), $r = r(p_T, \tau_{32}, \beta)$. The variable τ_{32} is not used for the low-mass analysis because it does not enhance the sensitivity of the search. In this case, the mistag rate is parametrized as a function of two variables only, using the same procedure. The mistag rate is binned, defined as $r_{i,j,k}$. To estimate the non-top-quark multijet background arising from mistagging light jets, a four-dimensional array of counts $N_{\alpha,i,j,k}$ is measured in the single t-tagged data sample, where α is the bin of the variable of interest (in this case, $M_{t\bar{t}}$), given by $N_{\alpha} = \sum_{a=1}^{N_{\text{jets}}} N_{\alpha,i,j,k} r_{i,j,k}$, where the indices i, j, k are the bins in p_T , τ_{32} , and β in which jet “a” lies. The four-dimensional parametrization properly accounts for correlated and uncorrelated statistical uncertainties. The uncertainty in each bin of the predicted mistagged distribution has two parts: one arises from the misidentification probability, and the other from the number of jets in the ensemble; they are uncorrelated and are added in quadrature. The details of this procedure are given in Appendix A.

Figure 7 shows the CA8 t tagging misidentification probability as a function of the CA8 jet p_T for different bins of τ_{32} and β . Figure 8 shows the CA15 t tagging misidentification probability as a function of the CA15 jet p_T for different values of β for the low-mass analysis. Figures 9 and 10 show validation of this procedure on QCD simulation in the various tagging categories for the high- and low-mass analysis, respectively. Good agreement between the predicted and selected contribution from QCD multijet production is observed in both analyses.

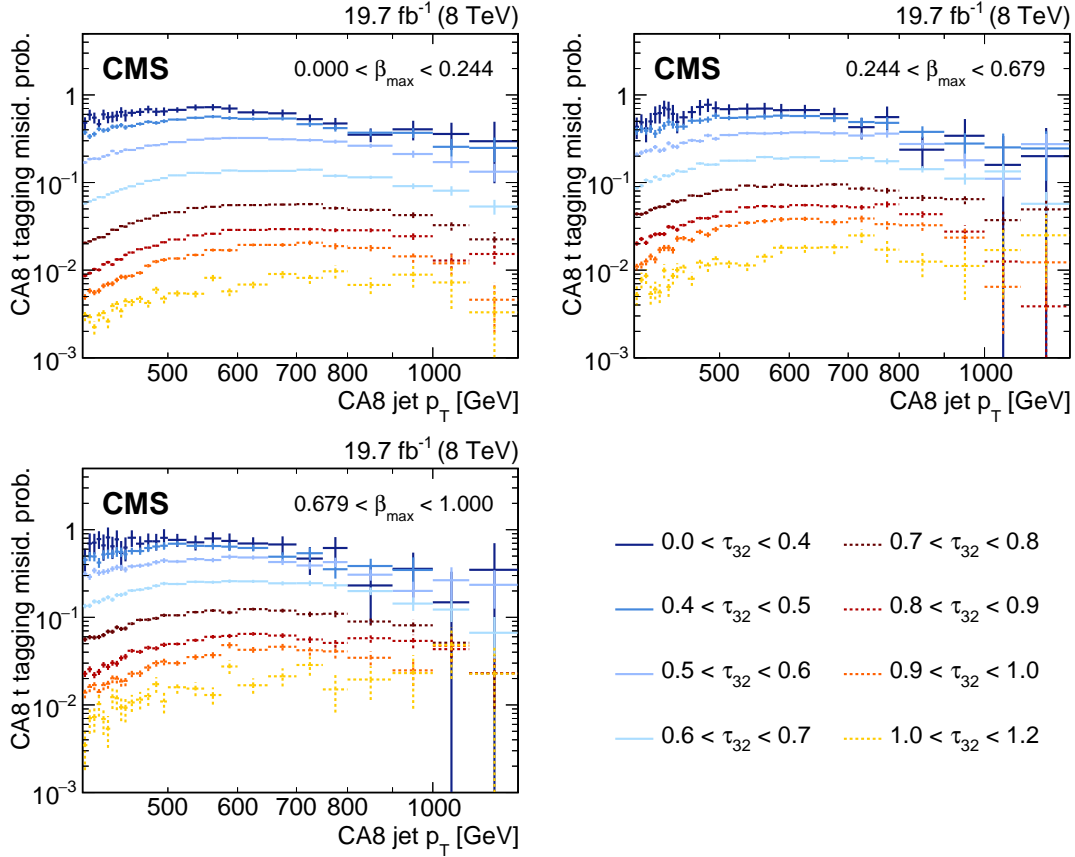


Figure 7: Misidentification probability for CA8 jets to be tagged as top-quark jets for different β ranges and for different τ_{32} values in the high-mass all-hadronic analysis. The horizontal error bars indicate the bin width.

The results of the high-mass selection in the all-hadronic channel are shown in Fig. 11 for events with $|\Delta y| < 1.0$ and $|\Delta y| > 1.0$ in the three b-tagged categories. The distributions of $M_{t\bar{t}}$ obtained with the low-mass selection are shown in Fig. 12 for events with two subjet b tags, for $H_T > 800$ GeV and $H_T < 800$ GeV. The $t\bar{t}$ background process is scaled by a factor derived from the maximum likelihood fit to data as explained in Section 7, and the non-top-quark multijet background is obtained from data in a sideband region.

6 Systematic uncertainties

The sources of systematic uncertainties considered in these analyses are summarized in Table 1. Uncertainties originating from the same source are assumed to be 100% correlated between all channels. The uncertainties can affect the normalization, the shape, or both normalization and shape of the $M_{t\bar{t}}$ distribution.

6.1 Uncertainties affecting the normalization

The following systematic uncertainties in the normalization of the background processes are considered. The uncertainty in the cross section for SM $t\bar{t}$ production is 15% [77]. Uncertainties in the production cross sections of W+jets are 9% for light-flavor jets [78] and 23% for heavy-flavor jets [79]. An uncertainty of 50% is assigned to the cross section of Z+jets production, obtained by varying the renormalization and factorization scales simultaneously by factors of

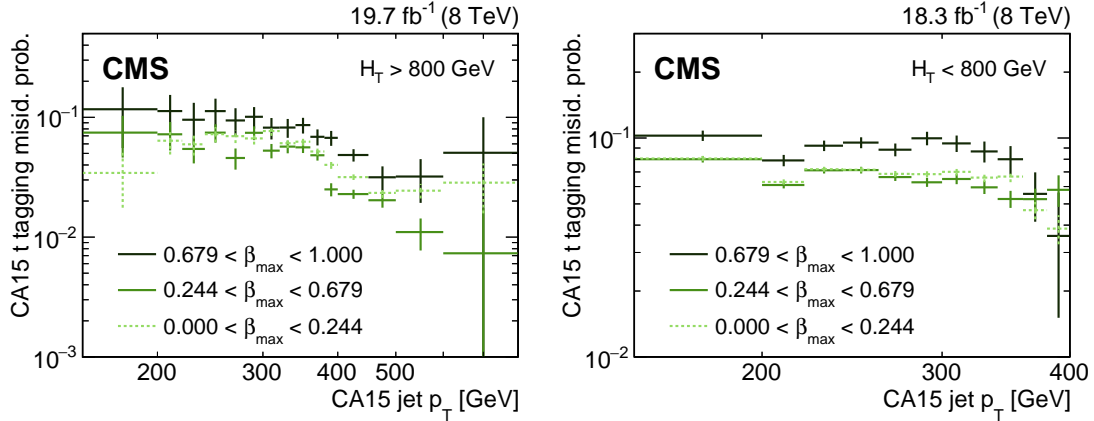


Figure 8: Misidentification probability for CA15 jets to be tagged as top-quark jets for different β values for $H_T > 800$ GeV (left) and $H_T < 800$ GeV (right) in the low-mass all-hadronic analysis. The horizontal error bars indicate the bin width.

0.5 and 2. The largest background contribution from single top quark production originates from the tW channel, which has been measured with an accuracy of 23% [80]; this uncertainty is used for all electroweak single top production processes. The uncertainty in diboson production is 20% [81, 82].

In addition, the following systematic uncertainties affect the normalization of all simulated processes, including signal processes. The uncertainty in the measurement of the integrated luminosity is 2.6% [83]. The combined trigger used in the electron category in the lepton+jets channel has an efficiency uncertainty of 1%. The uncertainty due to the single-muon trigger efficiency is 1%, which affects the muon category in the lepton+jets channel and the $e\mu$ and $\mu\mu$ categories in the dilepton channel.

6.2 Uncertainties affecting the shape

Systematic uncertainties due to the electron identification are applied as a function of electron p_T and η to events with an identified electron in the dilepton and lepton+jets channels. The uncertainty in the efficiency of the single electron trigger is applied as a function of electron p_T and η and affects the ee dilepton channel. Systematic uncertainties due to the muon identification and trigger efficiencies are applied as a function of muon p_T and η and affect events with a muon in the dilepton and lepton+jets channels.

The efficiencies of the H_T and four-jet triggers are measured as a function of H_T and the p_T of the fourth jet in the event, respectively. A correction is applied for the different behavior between data and simulation in the region where the triggers are not fully efficient. A systematic uncertainty of half the size of this correction is assigned, with a minimum of 2% in regions where the triggers are fully efficient as determined from MC studies of the efficiency. These uncertainties affect the all-hadronic analyses. Uncertainties in the jet energy scale and resolution are of the order of a few percent, and are functions of jet p_T and η . These are taken into account in all channels. These uncertainties are also propagated to the estimation of \vec{p}_T^{miss} . The systematic uncertainty associated with the pileup reweighting procedure is assumed to be fully correlated among all channels and is evaluated by varying the minimum bias cross section.

Efficiencies and mistag rates of the b tagging algorithm have been measured in data and simulated events for jets [47] and subjects with a spatial separation between them of $\Delta R > 0.3$ [56]. The corresponding uncertainty is correlated between the dilepton, lepton+jets, and the low-

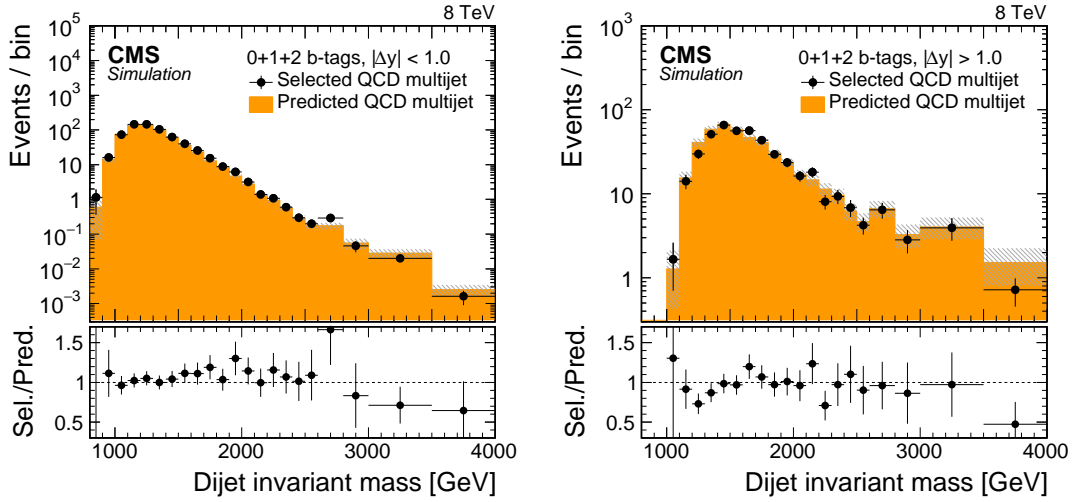


Figure 9: Results of the validation test for the high-mass all-hadronic analysis, using simulated QCD multijet events, to validate the data-driven background method used to estimate the QCD multijet contribution. Events are shown without any selection or division applied based on the number of identified b-tagged jets for $|\Delta y| < 1.0$ (left) and $|\Delta y| > 1.0$ (right). The points show the selected QCD multijet events in the signal region, with the horizontal error bars indicating the bin width. The solid histogram shows the predicted number of QCD multijet events using the misidentification probability for CA8 t-tagged jets measured in a statistically independent sideband region. The statistical uncertainty is shown as a shaded region. The ratio of selected to predicted events is shown in the bottom panel of each figure.

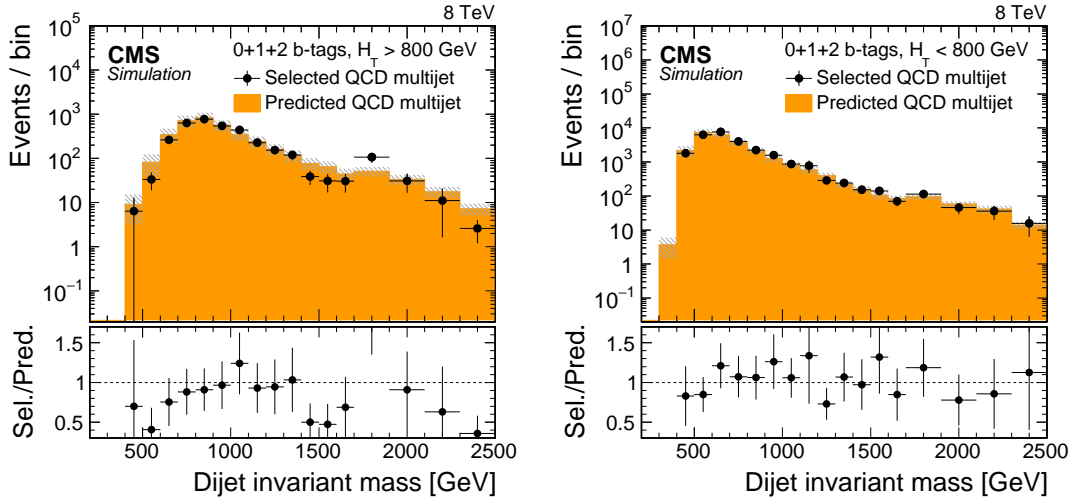


Figure 10: Results of the validation test for the low-mass all-hadronic analysis, using simulated QCD multijet events, to validate the data-driven background method used to estimate the QCD multijet contribution for events with $H_T > 800$ GeV (left), and events with $H_T < 800$ GeV (right). The points show the selected QCD multijet events in the signal region, with the horizontal error bars indicating the bin width. The solid histogram shows the predicted number of QCD multijet events using the misidentification probability for CA15 t-tagged jets measured in a statistically independent sideband region. The statistical uncertainty is shown as a shaded region. The ratio of selected to predicted events is shown in the bottom panel of each figure.

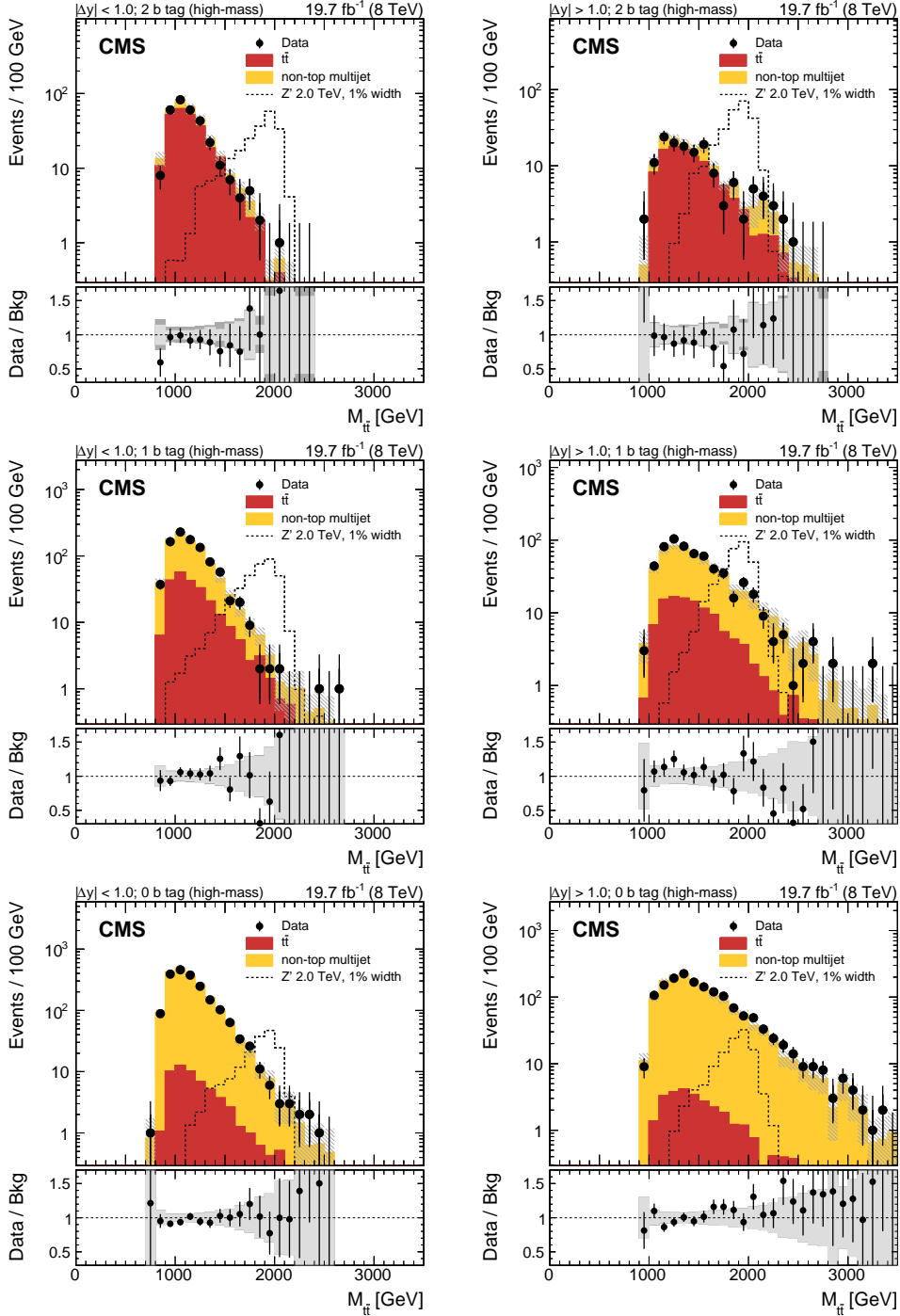


Figure 11: Reconstructed invariant mass of the $t\bar{t}$ pair in the all-hadronic channel for data and simulated events passing the high-mass selection. Events are divided into six categories: events with two subjet b-tags and $|\Delta y| < 1.0$ (upper left), one subjet btag and $|\Delta y| < 1.0$ (middle left), no subjet btag and $|\Delta y| < 1.0$ (lower left), two subjet btags and $|\Delta y| > 1.0$ (upper right), one subjet btag and $|\Delta y| > 1.0$ (middle right), no subjet btag and $|\Delta y| > 1.0$ (lower right). The uncertainty associated with the background expectation includes all the statistical and systematic uncertainties. For bins with no events in data but with non-zero background expectation, vertical lines are shown indicating the 68% confidence level coverage corresponding to an observation of zero events. The data-to-background ratio is shown in the bottom panel of each figure. For the ratio plot, the statistical uncertainty is shown in light gray, while the total uncertainty, which is the quadratic sum of the statistical and systematic uncertainties, is shown in dark gray. The expected distribution from a Z' signal with $M_{Z'} = 2 \text{ TeV}$ and $\Gamma_{Z'}/M_{Z'} = 0.01$ is also shown, normalized to a cross section of 1 pb .

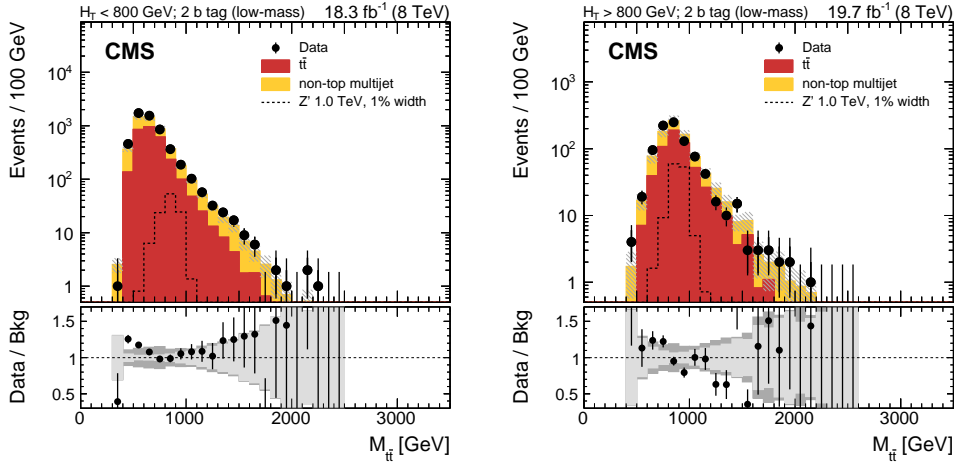


Figure 12: Reconstructed invariant mass of the $t\bar{t}$ pair in the all-hadronic channel for data and simulated events passing the low-mass selection. Events with two subjet b tags are shown, for $H_T < 800$ GeV (left) and $H_T > 800$ GeV (right). The signal is normalized to a cross section of 1 pb. The uncertainty associated with the background expectation includes all the statistical and systematic uncertainties. For bins with no events in data but with non-zero background expectation, vertical lines are shown indicating the 68% confidence level coverage corresponding to an observation of zero events. The data-to-background ratio is shown in the bottom panel of each figure. For the ratio plot, the statistical uncertainty is shown in light gray, while the total uncertainty, which is the quadratic sum of the statistical and systematic uncertainties, is shown in dark gray. The expected distribution from a Z' signal with $M_{Z'} = 1$ TeV and $\Gamma_{Z'}/M_{Z'} = 0.01$ is also shown, normalized to a cross section of 1 pb.

mass category of the all-hadronic channel. The high-mass selection in the all-hadronic channel uses subjet b tagging in a collimated region, where the subjets are separated by $\Delta R < 0.3$. The applicability of the standard b tagging correction factors and uncertainties is not guaranteed in this kinematic regime, because of double-counting of tracks from subjets, which are used in the b tagging algorithm. To account for this, the corresponding efficiency is measured simultaneously with the derivation of the cross section limits as described in Section 7, where the efficiency is left unconstrained in the maximum likelihood fit when deriving upper limits. This approach allows for a consistent extraction directly from the signal regions. The same procedure is used for the efficiency of the CA8 t tagging algorithm, combined with the requirement on τ_{32} .

The mistag rate of the CA8 t tagging algorithm has been studied for data and simulated events in a sideband region of the lepton+jets channel, dominated by W+jets events (as described in Section 5). An uncertainty of 25% is used for simulated events, which mostly affects the contribution of events from W+jets processes in events with one misidentified top-quark jet in the lepton+jets channel. Misidentified CA8 and CA15 t-tagged jets are the source of the QCD multijet background in the all-hadronic channel. The background estimation is obtained from data in sideband regions and the corresponding uncertainties are assumed to be fully uncorrelated between individual bins of the $M_{t\bar{t}}$ distribution. The efficiency of CA15 t-tagged jets has been studied in data and simulated events [51]. The associated uncertainty affects only the low-mass selection of the all-hadronic channel.

In addition to the experimental uncertainties, the following uncertainties affecting the predictions of the SM background processes are considered. The effect due to missing higher-orders in the simulation of SM processes is estimated by variations of the renormalization and factor-

ization scales. For the W +jets and $t\bar{t}$ simulated samples, the renormalization and factorization scales are varied simultaneously by factors of 0.5 or 2. The resulting uncertainty in continuum SM $t\bar{t}$ production affects all channels, while the uncertainty in W +jets production affects only the lepton+jets channel. The effect due to the uncertainty in extra hard-parton radiation is studied by varying the jet matching threshold for simulated W +jets processes by factors of 0.5 and 2. This uncertainty applies only to the lepton+jets channel. All simulated signal and background events are reweighted according to the uncertainties parametrized by the eigenvectors of the CTEQ6L and CT10 PDF sets. The shifts produced by the individual eigenvectors are added in quadrature in each bin of the $M_{t\bar{t}}$ distribution. The resulting uncertainty is taken to be fully correlated among all channels.

Table 1: Sources of systematic uncertainties and the channels they affect. The CA8 subjet b tagging uncertainty includes the uncertainties in both the efficiency and mistag rate. Uncorrelated uncertainties that apply to a given channel are marked by \odot . Uncertainties correlated between channels are marked by \oplus . The uncertainties listed in the upper part of the table are used in the evaluation of the background normalization.

Source of uncertainty	Prior uncertainty	2ℓ	ℓ +jets	Had. channel high-mass	Had. channel low-mass
Integrated luminosity	2.6%	\oplus	\oplus	\oplus	\oplus
$t\bar{t}$ cross section	15%	\oplus	\oplus	\oplus	\oplus
Single top quark cross section	23%	\oplus	\oplus		
Diboson cross section	20%	\oplus	\oplus		
Z+jets cross section	50%	\oplus	\oplus		
W +jets (light flavor) cross section	9%		\odot		
W +jets (heavy flavor) cross section	23%		\odot		
Electron+jet trigger	1%		\odot		
H_T trigger	2%			\oplus	\oplus
Four-jet trigger	$\pm 1\sigma(p_T)$				\odot
Single-electron trigger	$\pm 1\sigma(p_T, \eta)$	\odot			
Single-muon trigger and id	$\pm 1\sigma(p_T, \eta)$	\oplus	\oplus		
Electron ID	$\pm 1\sigma(p_T, \eta)$	\oplus	\oplus		
Jet energy scale	$\pm 1\sigma(p_T, \eta)$	\oplus	\oplus	\oplus	\oplus
Jet energy resolution	$\pm 1\sigma(\eta)$	\oplus	\oplus	\oplus	\oplus
Pileup uncertainty	$\pm 1\sigma$	\oplus	\oplus	\oplus	\oplus
b tagging efficiency ^(†)	$\pm 1\sigma(p_T, \eta)$	\oplus	\oplus		\oplus
b tagging mistag rate ^(†)	$\pm 1\sigma(p_T, \eta)$	\oplus	\oplus		\oplus
CA8 subjet b tagging	unconstrained			\odot	
CA8 t tagged jet efficiency	unconstrained		\oplus	\oplus	
CA8 t-tagged jet mistag	$\pm 25\%$		\odot		
CA15 t-tagged jet efficiency	$\pm 1\sigma(p_T, \eta)$				\odot
QCD multijet background	sideband			\odot	\odot
MC statistical uncertainty		\odot	\odot	\odot	\odot
PDF uncertainty	$\pm 1\sigma$	\oplus	\oplus	\oplus	\oplus
$t\bar{t}$ ren. and fact. scales	$4Q^2$ and $0.25Q^2$	\oplus	\oplus	\oplus	\oplus
W +jets ren. and fact. scales	$4Q^2$ and $0.25Q^2$		\odot		
W +jets matching scale μ	2μ and 0.5μ		\odot		

^(†) AK5 and CA15 subjets

The impact of the systematic uncertainties on the normalization of the total background depends strongly on the channel considered. The following uncertainties are the dominant ones in the two channels with the highest sensitivity, the category with one CA8 t-tagged jet in the

lepton+jets analysis and the category with two b-tagged jets in the high-mass all-hadronic analysis. The dominant uncertainty comes from missing higher orders in the simulation of the $t\bar{t}$ background and is on average 17%. The uncertainty due to the uncertainties in the PDFs is 15%, which is the same size as the uncertainty in the total $t\bar{t}$ cross section in the phase space considered. The size of other experimental uncertainties, like the CA8 t tagging efficiency, the subjet b tagging efficiency, and uncertainties due to the jet energy scale and resolution, vary between 4%–12%.

7 Estimation of the background normalization

The main source of irreducible background in all channels arises from SM $t\bar{t}$ production. In the lepton+jets channels, W +jets production contributes to events without a CA8 t-tagged jet. Single top quark, Z +jets, and diboson production constitute small backgrounds overall, and contribute to the dilepton and lepton+jets channels. In the following, these processes are combined into a single “others” category.

Except for the non-top-quark multijet backgrounds in the all-hadronic channels, the shapes of all SM backgrounds are estimated from simulation. The total yield of the simulated samples is obtained with a maximum likelihood fit to the $M_{t\bar{t}}$ distributions. Nuisance parameters are included in the fit to take into account the effect of systematic uncertainties. The parameters are constrained using log-normal probability density functions and are fitted simultaneously with the parameters corresponding to the background normalization.

Since there is no control sample of highly-boosted SM $t\bar{t}$ events that is disjoint from the signal regions of this analysis, the maximum likelihood fit is also used to extract the efficiency of the CA8 t tagging and subjet b tagging algorithms simultaneously. This is accomplished by separating the sample into subsamples based on the tagging criteria, and allowing the fit to find the best values for the nuisance parameters corresponding to these efficiencies. Higher-order calculations, as listed in Section 4, are used as prior assumptions on the cross sections of each background process, with the uncertainties discussed in Section 6. No assumption on the scale factor for the CA8 t-tagged jets is made and the corresponding nuisance parameter is left to float freely in the fit. The same is true for the subjet b tagging scale factor for the high-mass selection in the all-hadronic channel. This procedure effectively constrains the tagging efficiencies. No signal hypothesis is used in this procedure. Only the experimental uncertainties (see Section 6) are included in the likelihood fit. Uncertainties due to scale and matching systematics, as well as the uncertainties due to the PDF choice are not included. The list of uncertainties considered is given in the upper part of Table 1.

The fit converges with no parameter outside of two standard deviations of the prior assumption. A reduction of the uncertainty due to the $t\bar{t}$ normalization is obtained and a simultaneous measurement of the CA8 t tagging and subjet b tagging efficiencies is performed. These results do not change when including different signal hypotheses in the maximum likelihood fit.

The best fit values are used to scale the predictions for the various background processes. The measured CA8 t tagging efficiency is used to scale simulated events containing one CA8 t-tagged jet in the lepton+jets channel and all categories of the high-mass all-hadronic channels. The nuisance parameter for the subjet b tagging scale factor is used to scale all simulated events in the high-mass all-hadronic channels. The numerical values for the background normalization, the CA8 t tagging scale factor, and the subjet b tagging scale factor are given in Table 2, together with the prior and posterior uncertainties.

Table 2: Parameters for the background normalization of the given processes, the scale factor for CA8 t-tagged jets and the subset b tagging scale factor. The value of each parameter is obtained from a maximum likelihood fit. Also shown are the prior assumptions on the rate uncertainties and the posterior uncertainties obtained by the fit. In case of the subset b tagging scale factor, the best fit value and the posterior uncertainty are given in units of the standard b tagging scale factor and uncertainty.

Process	Best fit value	Prior uncertainty	Posterior uncertainty
$t\bar{t}$	0.99	15%	2.1%
W+jets (light flavor)	0.99	9%	5.0%
W+jets (c flavor)	1.06	23%	21%
W+jets (b flavor)	0.95	23%	18%
Single top quark	0.83	23%	22%
Z+jets	1.72	50%	36%
Diboson	1.02	20%	19%
CA8 t-tagged jets scale factor	0.94	unconstrained	3%
CA8 subset b tagging scale factor	1.3	unconstrained	1.5

The number of expected and observed events after the maximum likelihood estimation is shown in Tables 3–6 for all categories in the three channels.

8 Results

No significant excess of data over the expected SM background is observed. A Bayesian statistical method [84, 85] is used to derive 95% confidence level (CL) upper limits on the cross section times branching fraction for $Z' \rightarrow t\bar{t}$ production. The limits are derived employing a template based evaluation that uses the invariant mass distribution of the reconstructed $t\bar{t}$ pair. A likelihood fit is used to compare the signal and SM background expectations. To build the likelihood function, a Poisson probability is calculated in each bin of the mass distribution for each category in each channel. The parameters representing the Poisson mean of the signal strength and the background processes are determined in the fit. Pseudoexperiments are performed to extract expected limits under a background-only hypothesis. The systematic uncertainties discussed in Section 6 are taken into account through nuisance parameters. These are randomly varied within their ranges of validity using log normal distributions as the probability density function. Correlations between the systematic uncertainties across all channels are taken into account. The statistical uncertainties of simulated samples are treated as an additional Poisson nuisance parameter in each bin of the mass distribution.

The median of the distribution of the upper limits at 95% CL in the pseudoexperiments and the central 68% (95%) interval define the expected upper limit and $\pm 1\sigma$ ($\pm 2\sigma$) bands, respectively. Upper limits for three benchmark signal hypotheses are calculated: a topcolor Z' boson [10] with relative widths $\Gamma_{Z'}/M_{Z'} = 1.0\%$ or $\Gamma_{Z'}/M_{Z'} = 10\%$, and a Randall–Sundrum KK gluon with coupling as described in Ref. [18]. Resonance masses between 0.75 and 3 TeV are considered using simulated samples with mass values given in Section 4. Above mass values of 3 TeV, narrow-width signals would have cross sections below 1 fb, placing them beyond the reach of

Table 3: Signal efficiency and number of events in the ee , $e\mu$, and $\mu\mu$ channels. The yield of each MC background is obtained from NLO+NNLL calculations, multiplied by a scale factor derived from the likelihood fit. The uncertainty given for each background process includes the MC statistical uncertainty added in quadrature with all systematic uncertainties. The resonance relative decay width $\Gamma_{Z'}/M_{Z'}$ is indicated by w .

	ee channel	$e\mu$ channel	$\mu\mu$ channel
	Efficiency		
Z' ($M = 1$ TeV, $w = 1\%$)	0.22%	0.47%	0.28%
Z' ($M = 2$ TeV, $w = 1\%$)	0.34%	0.84%	0.55%
Z' ($M = 3$ TeV, $w = 1\%$)	0.25%	0.61%	0.54%
Z' ($M = 1$ TeV, $w = 10\%$)	0.18%	0.44%	0.28%
Z' ($M = 2$ TeV, $w = 10\%$)	0.31%	0.69%	0.49%
Z' ($M = 3$ TeV, $w = 10\%$)	0.27%	0.60%	0.37%
g_{KK} ($M = 1$ TeV)	0.18%	0.41%	0.21%
g_{KK} ($M = 2$ TeV)	0.25%	0.51%	0.35%
g_{KK} ($M = 3$ TeV)	0.16%	0.42%	0.28%
	Number of events		
$t\bar{t}$	834 ± 43	2955 ± 148	1696 ± 86
Single top quark	25 ± 7	67 ± 18	40 ± 11
Z+jets	39 ± 23	9 ± 8	158 ± 82
Diboson	1 ± 1	2 ± 1	3 ± 1
Total background	898 ± 67	3032 ± 167	1897 ± 170
Data	832	3006	1813

Table 4: Signal efficiency and number of events in the e+jets and μ +jets channels. The yield of each MC background is obtained from NLO+NNLL calculations, multiplied by a scale factor derived from the likelihood fit. The uncertainty given for each background process includes the MC statistical uncertainty added in quadrature with all systematic uncertainties. The resonance relative decay width $\Gamma_{Z'}/M_{Z'}$ is indicated by w .

	e+jets channel			μ +jets channel		
	0-t, 0-b	0-t, 1-b	1-t	0-t, 0-b	0-t, 1-b	1-t
	Efficiency					
Z' ($M = 1$ TeV, $w = 1\%$)	0.5%	2.3%	0.5%	0.4%	2.2%	0.4%
Z' ($M = 2$ TeV, $w = 1\%$)	1.1%	2.5%	2.4%	1.1%	2.4%	2.3%
Z' ($M = 3$ TeV, $w = 1\%$)	1.5%	2.3%	1.8%	1.7%	2.3%	2.0%
Z' ($M = 1$ TeV, $w = 10\%$)	0.5%	2.1%	0.4%	0.4%	2.1%	0.4%
Z' ($M = 2$ TeV, $w = 10\%$)	0.9%	2.3%	1.9%	0.9%	2.2%	1.8%
Z' ($M = 3$ TeV, $w = 10\%$)	0.9%	2.1%	1.4%	1.0%	1.8%	1.4%
g_{KK} ($M = 1$ TeV)	0.5%	1.8%	0.3%	0.4%	1.8%	0.3%
g_{KK} ($M = 2$ TeV)	0.7%	1.9%	1.3%	0.7%	1.8%	1.2%
g_{KK} ($M = 3$ TeV)	0.6%	1.5%	0.8%	0.6%	1.4%	0.9%
	Number of events					
$t\bar{t}$	3127 ± 254	11345 ± 796	499 ± 47	3322 ± 255	11634 ± 749	491 ± 49
W+jets (light flavor)	4790 ± 955	222 ± 57	30 ± 9	4891 ± 875	207 ± 50	29 ± 8
W+jets (c flavor)	1128 ± 397	303 ± 110	8 ± 4	1186 ± 405	333 ± 117	11 ± 5
W+jets (b flavor)	111 ± 33	250 ± 76	3 ± 1	102 ± 29	243 ± 70	2 ± 1
Single top quark	244 ± 63	667 ± 169	8 ± 3	238 ± 61	702 ± 178	8 ± 3
Z+jets	485 ± 123	90 ± 23	3 ± 1	606 ± 153	110 ± 28	4 ± 1
Diboson	123 ± 25	29 ± 6	1 ± 1	134 ± 27	27 ± 6	1 ± 1
Total background	10007 ± 1422	12906 ± 1062	552 ± 53	10479 ± 1407	13256 ± 1049	545 ± 54
Data	10204	12157	465	10099	12510	493

Table 5: Signal efficiency and number of events in the high-mass all-hadronic channel. The yield of the $t\bar{t}$ background is obtained from NLO+NNLL calculations, multiplied by a scale factor derived from the likelihood fit. The multijet background is obtained from sideband regions in data. The uncertainty given for each background process includes the statistical uncertainty added in quadrature with all systematic uncertainties. The resonance relative decay width $\Gamma_{Z'}/M_{Z'}$ is indicated by w .

	$ \Delta y < 1.0$			$ \Delta y > 1.0$		
	0 b-tag	1 b-tag	2 b-tags	0 b-tag	1 b-tag	2 b-tags
	Efficiency					
Z' ($M = 1 \text{ TeV}, w = 1\%$)	0.1%	0.3%	0.4%	0.0%	0.0%	0.0%
Z' ($M = 2 \text{ TeV}, w = 1\%$)	0.8%	1.8%	1.1%	0.6%	1.7%	1.3%
Z' ($M = 3 \text{ TeV}, w = 1\%$)	0.6%	1.0%	0.4%	0.8%	1.6%	0.9%
Z' ($M = 1 \text{ TeV}, w = 10\%$)	0.1%	0.3%	0.4%	0.0%	0.0%	0.0%
Z' ($M = 2 \text{ TeV}, w = 10\%$)	0.6%	1.6%	1.0%	0.3%	1.3%	0.9%
Z' ($M = 3 \text{ TeV}, w = 10\%$)	0.4%	0.9%	0.5%	0.4%	0.9%	0.6%
g_{KK} ($M = 1 \text{ TeV}$)	0.1%	0.2%	0.2%	0.0%	0.0%	0.0%
g_{KK} ($M = 2 \text{ TeV}$)	0.3%	1.0%	0.8%	0.2%	0.7%	0.6%
g_{KK} ($M = 3 \text{ TeV}$)	0.2%	0.6%	0.4%	0.2%	0.5%	0.4%
	Number of events					
$t\bar{t}$	59 ± 11	243 ± 30	262 ± 32	29 ± 5	112 ± 11	109 ± 12
QCD multijet	1984 ± 68	678 ± 31	68 ± 8	1465 ± 54	456 ± 24	41 ± 7
Total background	2043 ± 70	921 ± 46	330 ± 33	1493 ± 55	568 ± 28	150 ± 14
Data	1956	933	305	1523	604	143

Table 6: Signal efficiency and number of events in the low-mass all-hadronic channel. The yield of the $t\bar{t}$ background is obtained from NLO+NNLL calculations, multiplied by a scale factor derived from the likelihood fit. The multijet background is obtained from sideband regions in data. The uncertainty given for each background process includes the statistical uncertainty added in quadrature with all systematic uncertainties. The resonance relative decay width $\Gamma_{Z'}/M_{Z'}$ is indicated by w .

	$H_T < 800 \text{ GeV}$			$H_T > 800 \text{ GeV}$		
	0 b-tag	1 b-tag	2 b-tags	0 b-tag	1 b-tag	2 b-tags
	Efficiency					
$Z' (M = 0.75 \text{ TeV}, w = 1\%)$	0.17%	0.64%	0.70%	0.01%	0.04%	0.03%
$Z' (M = 1 \text{ TeV}, w = 1\%)$	0.13%	0.54%	0.56%	0.16%	0.61%	0.66%
$Z' (M = 2 \text{ TeV}, w = 1\%)$	0.04%	0.09%	0.07%	0.08%	0.26%	0.18%
$Z' (M = 0.75 \text{ TeV}, w = 10\%)$	0.15%	0.62%	0.64%	0.01%	0.06%	0.05%
$Z' (M = 1 \text{ TeV}, w = 10\%)$	0.12%	0.54%	0.54%	0.13%	0.49%	0.50%
$Z' (M = 2 \text{ TeV}, w = 10\%)$	0.04%	0.18%	0.15%	0.07%	0.27%	0.21%
$g_{KK} (M = 0.7 \text{ TeV})$	0.11%	0.37%	0.42%	0.01%	0.04%	0.04%
$g_{KK} (M = 1 \text{ TeV})$	0.11%	0.47%	0.49%	0.08%	0.40%	0.32%
$g_{KK} (M = 2 \text{ TeV})$	0.06%	0.24%	0.19%	0.07%	0.23%	0.21%
	Number of events					
$t\bar{t}$	851 ± 216	3238 ± 716	3009 ± 644	196 ± 65	698 ± 203	583 ± 165
QCD multijet	55932 ± 1598	18687 ± 613	1933 ± 92	8544 ± 331	3080 ± 168	311 ± 30
Total background	56781 ± 1633	21926 ± 984	4942 ± 655	8740 ± 341	3778 ± 268	894 ± 168
Data	57118	22485	5381	8920	3935	891

Run 1 at the LHC, and signals with relative widths larger than 10% would show no resonance structure at the collision energy of 8 TeV. All limits are given at 95% CL.

A comparison of the expected limits obtained from the individual channels is shown in Fig. 13. Also shown are the results from a search optimized for threshold production of the $t\bar{t}$ pair in the lepton+jets channel [31]. This channel has the best sensitivity for resonance masses below 0.75 TeV. Above this value, the combination of the boosted analyses described in this paper places better limits on the production cross section times branching fraction. The best overall sensitivity is obtained in the lepton+jets channel. The high-mass selection of the all-hadronic channel has comparable sensitivity in the mass region above 2 TeV.

Figure 14 shows the results for each of the three signal hypotheses. The cross section limits for the narrow signal hypothesis are compared to the cross section for the production of a Z' boson with 1.2% width. This width is chosen for comparison with theoretical results and previous measurements. Resonances with masses up to 2.4 TeV (2.4 TeV expected) for the narrow Z' hypothesis are excluded. These cross section limits are model independent, meaning that they are valid for any resonance decaying to $t\bar{t}$, with a width well below the experimental resolution of about 10%. Wide resonances with 10% width are excluded up to 2.9 TeV (2.8 TeV expected). The better limits with respect to narrow resonances are due to the higher production cross section of the wider Z' resonance. Randall–Sundrum KK gluons decaying to $t\bar{t}$ are excluded with masses below 2.8 TeV (2.7 TeV expected). This model exhibits the weakest upper limits on the production cross section, because of the long tails towards low resonance masses present in the predicted $M_{t\bar{t}}$ distribution. These tails are introduced by the interplay between the large natural width of the KK gluons and the parton luminosity, causing masses that are far below the resonance mass to have a larger probability than events near the resonance itself. The expected and observed exclusion limits for different resonance masses are given in Table 7.

The upper limits on the production cross section times branching fraction into $t\bar{t}$ are given in Table 8, for different resonance masses. The upper limits on the cross sections show improvements of about 50% with respect to a previous combination of results from a search in the lepton+jets and all-hadronic channels [31]. These improvements are mostly due to the use of t tagging in the lepton+jets channel, and the application of b tagging on subjets in the all-

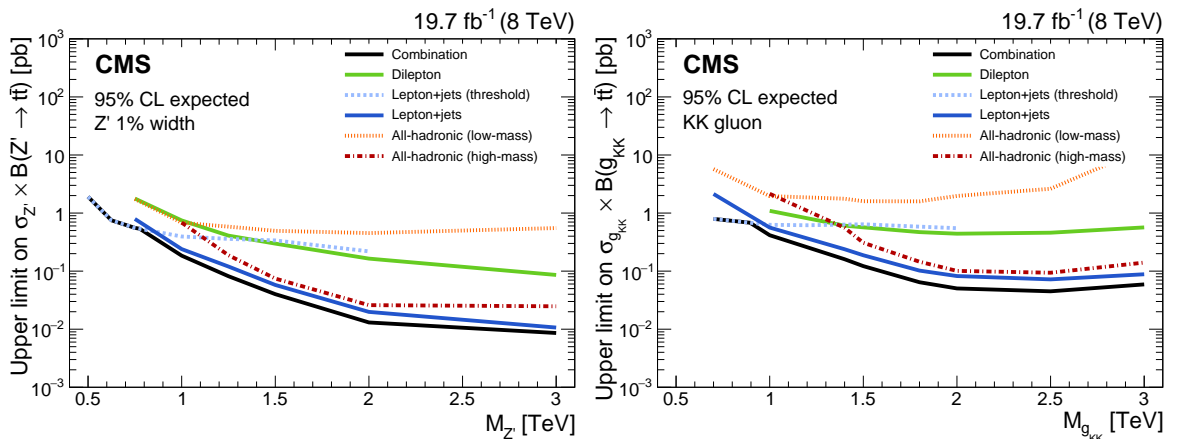


Figure 13: Expected 95% CL upper limits on the production cross section times branching fraction for a Z' boson decaying to $t\bar{t}$ with 1% width (left) and a KK gluon in the RS model (right). The limits obtained from the individual channels are shown separately, together with the result from the combination. Also shown are results from a threshold analysis in the lepton+jets channel [31], optimized for low mass values.

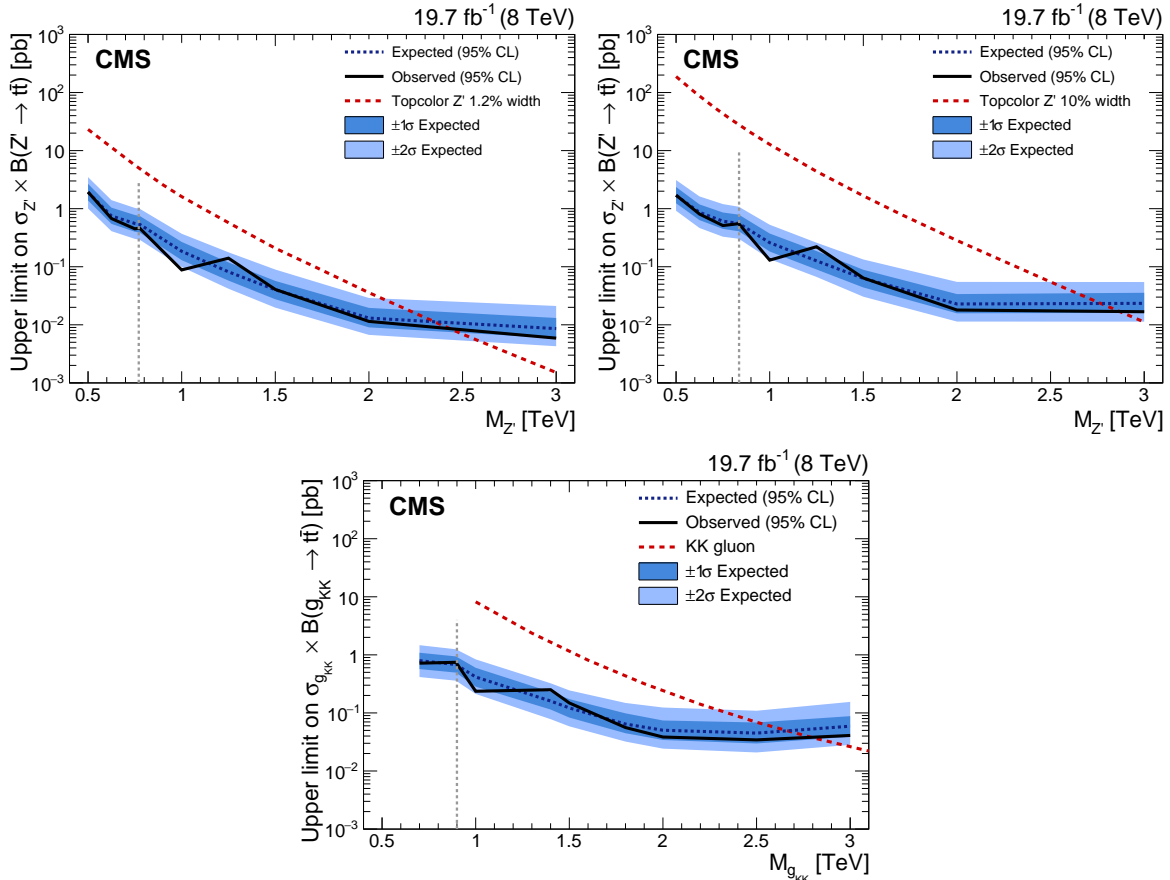


Figure 14: Upper limits at 95% CL on the production cross section times branching fraction for a Z' boson decaying to $t\bar{t}$ with narrow width (upper left), with 10% width (upper right) and a KK gluon in the Randall–Sundrum model decaying to $t\bar{t}$ (bottom). The vertical dashed line indicates the transition from a threshold analysis [31] to the combination, in providing the best expected limit. Below this dashed line, only the results of the low-mass analysis with resolved jets are quoted; above this line, the results from the combination of the boosted channels are given. The limits are shown as a function of the resonance mass and are compared to predictions for the cross section of a Z' boson with relative width of 1.2% and 10% [10] and the prediction for the production of a KK gluon [18]. The predictions are multiplied by a factor of 1.3 to account for higher-order corrections [69].

Table 7: Expected and observed lower mass limits for the three benchmark models. Mass limits are given for the dilepton analysis, the lepton+jets analysis, the combination of the two all-hadronic analyses and the full combination of all four analyses. All limits are given at 95% CL.

	Mass limit [TeV]							
	Dilepton channel		Lepton+jets channel		All-hadronic channels		Combined	
	Expected	Observed	Expected	Observed	Expected	Observed	Expected	Observed
$Z', \Gamma_{Z'}/M_{Z'} = 1.2\%$	1.4	1.5	2.2	2.3	2.1	2.1	2.4	2.4
$Z', \Gamma_{Z'}/M_{Z'} = 10\%$	2.1	2.2	2.7	2.8	2.5	2.5	2.8	2.9
RS KK gluon	1.8	2.0	2.5	2.5	2.4	2.3	2.7	2.8

Table 8: Expected and observed limits for the production cross section times branching fraction of a Z' boson decaying to $t\bar{t}$ with a width of 1%, 10% and a KK gluon in the RS model. All limits are given at 95% CL.

		$Z', \Gamma_{Z'}/M_{Z'} = 1\%$					
$M_{Z'}$ (TeV)	Expected (pb)	Expected range ($\pm 1\sigma$) (pb)		Expected range ($\pm 2\sigma$) (pb)		Observed (pb)	
0.75	0.61	0.89	— 0.43	1.3	— 0.32	0.86	
1.0	0.18	0.27	— 0.13	0.37	— 0.099	0.088	
1.25	0.082	0.12	— 0.058	0.18	— 0.042	0.14	
1.5	0.04	0.057	— 0.028	0.089	— 0.02	0.041	
2.0	0.013	0.02	— 0.009	0.029	— 0.0067	0.011	
3.0	0.0086	0.013	— 0.0059	0.021	— 0.0043	0.0059	
		$Z', \Gamma_{Z'}/M_{Z'} = 10\%$					
$M_{Z'}$ (TeV)	Expected (pb)	Expected range ($\pm 1\sigma$) (pb)		Expected range ($\pm 2\sigma$) (pb)		Observed (pb)	
0.75	0.83	1.2	— 0.57	1.8	— 0.42	0.89	
1.0	0.26	0.37	— 0.18	0.53	— 0.14	0.13	
1.25	0.13	0.19	— 0.09	0.26	— 0.067	0.22	
1.5	0.063	0.089	— 0.044	0.13	— 0.03	0.064	
2.0	0.023	0.034	— 0.016	0.055	— 0.011	0.018	
3.0	0.023	0.036	— 0.016	0.055	— 0.011	0.017	
		RS KK gluon					
$M_{g_{KK}}$ (TeV)	Expected (pb)	Expected range ($\pm 1\sigma$) (pb)		Expected range ($\pm 2\sigma$) (pb)		Observed (pb)	
0.7	1.7	2.5	— 1.2	3.8	— 0.84	3.5	
1.0	0.42	0.6	— 0.28	0.84	— 0.21	0.24	
1.4	0.16	0.23	— 0.11	0.32	— 0.078	0.25	
1.5	0.12	0.17	— 0.083	0.24	— 0.059	0.15	
1.8	0.064	0.098	— 0.045	0.15	— 0.032	0.056	
2.0	0.05	0.074	— 0.034	0.12	— 0.024	0.038	
2.5	0.045	0.068	— 0.03	0.11	— 0.021	0.034	
3.0	0.059	0.088	— 0.039	0.15	— 0.028	0.041	

hadronic channel. The limits for $M_{Z'} < 1$ TeV are improved with the addition of the dilepton channel and the low-mass selection in the all-hadronic channel.

9 Summary

A search has been performed for the production of heavy $t\bar{t}$ resonances in final states including two, one, or no leptons. The analysis is based on a data sample corresponding to an integrated luminosity of 19.7 fb^{-1} recorded in 2012 with the CMS detector in proton-proton collisions at $\sqrt{s} = 8$ TeV at the LHC. No evidence is found for a resonant $t\bar{t}$ component beyond the standard model $t\bar{t}$ continuum production. Model-independent cross section limits are set on the production of such resonances that have widths well below the experimental resolution of about 10%.

Cross sections times branching fractions above 11 fb are excluded at 95% confidence level (CL) for the process $pp \rightarrow Z' \rightarrow t\bar{t}$ with a Z' resonance [10] with mass of 2 TeV and width $\Gamma_{Z'}/M_{Z'} = 1\%$. The corresponding 95% CL expected cross section limit is 13 fb. The 95% CL observed lower mass limit for a topcolor narrow Z' resonance with $\Gamma_{Z'}/M_{Z'} = 1.2\%$ corresponds to 2.4 TeV, which agrees with the expected limit.

Observed and expected 95% CL upper limits of 18 fb (23 fb) are set for a Z' boson [10] with a mass of 2 TeV and width $\Gamma_{Z'}/M_{Z'} = 10\%$. The respective 95% CL observed and expected lower mass limits are 2.9 and 2.8 TeV for a wide topcolor Z' resonance.

For the production of Kaluza–Klein gluon excitations $pp \rightarrow g_{KK} \rightarrow t\bar{t}$ predicted in Randall–Sundrum models [18], an upper limit on the cross section of 38 fb is observed (50 fb expected) at 95% CL for a mass of 2 TeV. The observed and expected lower mass limits are 2.8 and 2.7 TeV.

These mass limits represent significant improvements over previous ones set at $\sqrt{s} = 7$ TeV [26, 29, 30]. An improvement by about 50% on the 95% CL upper limits with respect to an earlier search optimized for high masses at $\sqrt{s} = 8$ TeV [31] is achieved by the application of additional jet substructure information and the addition of the dilepton channel. The results presented provide the most stringent constraints on resonant $t\bar{t}$ production to date.

Acknowledgments

We congratulate our colleagues in the CERN accelerator departments for the excellent performance of the LHC and thank the technical and administrative staffs at CERN and at other CMS institutes for their contributions to the success of the CMS effort. In addition, we gratefully acknowledge the computing centers and personnel of the Worldwide LHC Computing Grid for delivering so effectively the computing infrastructure essential to our analyses. Finally, we acknowledge the enduring support for the construction and operation of the LHC and the CMS detector provided by the following funding agencies: the Austrian Federal Ministry of Science, Research and Economy and the Austrian Science Fund; the Belgian Fonds de la Recherche Scientifique, and Fonds voor Wetenschappelijk Onderzoek; the Brazilian Funding Agencies (CNPq, CAPES, FAPERJ, and FAPESP); the Bulgarian Ministry of Education and Science; CERN; the Chinese Academy of Sciences, Ministry of Science and Technology, and National Natural Science Foundation of China; the Colombian Funding Agency (COLCIENCIAS); the Croatian Ministry of Science, Education and Sport, and the Croatian Science Foundation; the Research Promotion Foundation, Cyprus; the Ministry of Education and Research, Estonian Research Council via IUT23-4 and IUT23-6 and European Regional Development Fund, Estonia; the Academy of Finland, Finnish Ministry of Education and Culture, and Helsinki

Institute of Physics; the Institut National de Physique Nucléaire et de Physique des Particules / CNRS, and Commissariat à l'Énergie Atomique et aux Énergies Alternatives / CEA, France; the Bundesministerium für Bildung und Forschung, Deutsche Forschungsgemeinschaft, and Helmholtz-Gemeinschaft Deutscher Forschungszentren, Germany; the General Secretariat for Research and Technology, Greece; the National Scientific Research Foundation, and National Innovation Office, Hungary; the Department of Atomic Energy and the Department of Science and Technology, India; the Institute for Studies in Theoretical Physics and Mathematics, Iran; the Science Foundation, Ireland; the Istituto Nazionale di Fisica Nucleare, Italy; the Korean Ministry of Education, Science and Technology and the World Class University program of NRF, Republic of Korea; the Lithuanian Academy of Sciences; the Ministry of Education, and University of Malaya (Malaysia); the Mexican Funding Agencies (CINVESTAV, CONACYT, SEP, and UASLP-FAI); the Ministry of Business, Innovation and Employment, New Zealand; the Pakistan Atomic Energy Commission; the Ministry of Science and Higher Education and the National Science Centre, Poland; the Fundação para a Ciência e a Tecnologia, Portugal; JINR, Dubna; the Ministry of Education and Science of the Russian Federation, the Federal Agency of Atomic Energy of the Russian Federation, Russian Academy of Sciences, and the Russian Foundation for Basic Research; the Ministry of Education, Science and Technological Development of Serbia; the Secretaría de Estado de Investigación, Desarrollo e Innovación and Programa Consolider-Ingenio 2010, Spain; the Swiss Funding Agencies (ETH Board, ETH Zurich, PSI, SNF, UniZH, Canton Zurich, and SER); the Ministry of Science and Technology, Taipei; the Thailand Center of Excellence in Physics, the Institute for the Promotion of Teaching Science and Technology of Thailand, Special Task Force for Activating Research and the National Science and Technology Development Agency of Thailand; the Scientific and Technical Research Council of Turkey, and Turkish Atomic Energy Authority; the National Academy of Sciences of Ukraine, and State Fund for Fundamental Researches, Ukraine; the Science and Technology Facilities Council, UK; the US Department of Energy, and the US National Science Foundation.

Individuals have received support from the Marie-Curie programme and the European Research Council and EPLANET (European Union); the Leventis Foundation; the A. P. Sloan Foundation; the Alexander von Humboldt Foundation; the Belgian Federal Science Policy Office; the Fonds pour la Formation à la Recherche dans l'Industrie et dans l'Agriculture (FRIA-Belgium); the Agentschap voor Innovatie door Wetenschap en Technologie (IWT-Belgium); the Ministry of Education, Youth and Sports (MEYS) of the Czech Republic; the Council of Science and Industrial Research, India; the HOMING PLUS programme of Foundation for Polish Science, cofinanced from European Union, Regional Development Fund; the Compagnia di San Paolo (Torino); the Thalís and Aristeia programmes cofinanced by EU-ESF and the Greek NSRF; and the National Priorities Research Program by Qatar National Research Fund.

References

- [1] ATLAS Collaboration, "Observation of a new particle in the search for the Standard Model Higgs boson with the ATLAS detector at the LHC", *Phys. Lett. B* **716** (2012) 1, doi:10.1016/j.physletb.2012.08.020, arXiv:1207.7214.
- [2] CMS Collaboration, "Observation of a new boson at a mass of 125 GeV with the CMS experiment at the LHC", *Phys. Lett. B* **716** (2012) 30, doi:10.1016/j.physletb.2012.08.021, arXiv:1207.7235.
- [3] CMS Collaboration, "Observation of a new boson with mass near 125 GeV in pp collisions at $\sqrt{s} = 7$ and 8 TeV", *JHEP* **06** (2013) 081, doi:10.1007/JHEP06(2013)081, arXiv:1303.4571.
- [4] ATLAS Collaboration, "Measurement of the Higgs boson mass from the $H \rightarrow \gamma\gamma$ and $H \rightarrow ZZ^* \rightarrow 4\ell$ channels with the ATLAS detector using 25 fb⁻¹ of pp collision data", *Phys. Rev. D* **90** (2014) 052004, doi:10.1103/PhysRevD.90.052004, arXiv:1406.3827.
- [5] CMS Collaboration, "Precise determination of the mass of the Higgs boson and tests of compatibility of its couplings with the standard model predictions using proton collisions at 7 and 8 TeV", *Eur. Phys. J. C* **75** (2015) 212, doi:10.1140/epjc/s10052-015-3351-7, arXiv:1412.8662.
- [6] ATLAS, CMS Collaboration, "Combined Measurement of the Higgs Boson Mass in pp Collisions at $\sqrt{s} = 7$ and 8 TeV with the ATLAS and CMS Experiments", *Phys. Rev. Lett.* **114** (2015) 191803, doi:10.1103/PhysRevLett.114.191803, arXiv:1503.07589.
- [7] C. T. Hill, "Topcolor: Top quark condensation in a gauge extension of the standard model", *Phys. Lett. B* **266** (1991) 419, doi:10.1016/0370-2693(91)91061-Y.
- [8] C. T. Hill and S. J. Parke, "Top production: Sensitivity to new physics", *Phys. Rev. D* **49** (1994) 4454, doi:10.1103/PhysRevD.49.4454, arXiv:hep-ph/9312324.
- [9] C. T. Hill, "Topcolor assisted technicolor", *Phys. Lett. B* **345** (1995) 483, doi:10.1016/0370-2693(94)01660-5, arXiv:hep-ph/9411426. Updates in arXiv:hep-ph/9911288.
- [10] R. M. Harris and S. Jain, "Cross sections for leptophobic topcolor Z' decaying to top-antitop", *Eur. Phys. J. C* **72** (2012) 2072, doi:10.1140/epjc/s10052-012-2072-4, arXiv:1112.4928.
- [11] J. L. Rosner, "Prominent decay modes of a leptophobic Z' ", *Phys. Lett. B* **387** (1996) 113, doi:10.1016/0370-2693(96)01022-2, arXiv:hep-ph/9607207.
- [12] K. R. Lynch, S. Mrenna, M. Narain, and E. H. Simmons, "Finding Z' bosons coupled preferentially to the third family at CERN LEP and the Fermilab Tevatron", *Phys. Rev. D* **63** (2001) 035006, doi:10.1103/PhysRevD.63.035006, arXiv:hep-ph/0007286.
- [13] M. Carena, A. Daleo, B. A. Dobrescu, and T. M. P. Tait, " Z' gauge bosons at the Fermilab Tevatron", *Phys. Rev. D* **70** (2004) 093009, doi:10.1103/PhysRevD.70.093009, arXiv:hep-ph/0408098.
- [14] P. H. Frampton and S. L. Glashow, "Chiral color: An alternative to the standard model", *Phys. Lett. B* **190** (1987) 157, doi:10.1016/0370-2693(87)90859-8.

- [15] D. Choudhurya, R. M. Godbole, R. K. Singh, and K. Wagh, "Top production at the Tevatron/LHC and nonstandard, strongly interacting spin one particles", *Phys. Lett. B* **657** (2007) 69, doi:10.1016/j.physletb.2007.09.057, arXiv:0705.1499. Updates in arXiv:0810.3635.
- [16] D. Dicus, A. Stange, and S. Willenbrock, "Higgs decay to top quarks at hadron colliders", *Phys. Lett. B* **333** (1994) 126, doi:10.1016/0370-2693(94)91017-0, arXiv:hep-ph/9404359.
- [17] L. Randall and R. Sundrum, "A large mass hierarchy from a small extra dimension", *Phys. Rev. Lett.* **83** (1999) 3370, doi:10.1103/PhysRevLett.83.3370, arXiv:hep-ph/9905221.
- [18] K. Agashe et al., "LHC signals from warped extra dimensions", *Phys. Rev. D* **77** (2008) 015003, doi:10.1103/PhysRevD.77.015003, arXiv:hep-ph/0612015.
- [19] H. Davoudiasl, J. L. Hewett, and T. G. Rizzo, "Phenomenology of the Randall-Sundrum Gauge Hierarchy Model", *Phys. Rev. Lett.* **84** (2000) 2080, doi:10.1103/PhysRevLett.84.2080, arXiv:hep-ph/9909255.
- [20] CDF Collaboration, "Limits on the production of narrow $t\bar{t}$ resonances in $p\bar{p}$ collisions at $\sqrt{s} = 1.96$ TeV", *Phys. Rev. D* **77** (2008) 051102, doi:10.1103/PhysRevD.77.051102, arXiv:0710.5335.
- [21] CDF Collaboration, "Search for resonant $t\bar{t}$ production in $p\bar{p}$ collisions at $\sqrt{s} = 1.96$ TeV", *Phys. Rev. Lett.* **100** (2008) 231801, doi:10.1103/PhysRevLett.100.231801, arXiv:0709.0705.
- [22] CDF Collaboration, "A Search for resonant production of $t\bar{t}$ pairs in 4.8 fb^{-1} of integrated luminosity of $p\bar{p}$ collisions at $\sqrt{s} = 1.96$ TeV", *Phys. Rev. D* **84** (2011) 072004, doi:10.1103/PhysRevD.84.072004, arXiv:1107.5063.
- [23] D0 Collaboration, "Search for a narrow $t\bar{t}$ resonance in $p\bar{p}$ collisions at $\sqrt{s} = 1.96$ TeV", *Phys. Rev. D* **85** (2012) 051101, doi:10.1103/PhysRevD.85.051101, arXiv:1111.1271.
- [24] CDF Collaboration, "Search for resonant production of $t\bar{t}$ decaying to jets in $p\bar{p}$ collisions at $\sqrt{s} = 1.96$ TeV", *Phys. Rev. D* **84** (2011) 072003, doi:10.1103/PhysRevD.84.072003, arXiv:1108.4755.
- [25] D0 Collaboration, "Search for $t\bar{t}$ resonances in the lepton plus jets final state in $p\bar{p}$ collisions at $\sqrt{s} = 1.96$ TeV", *Phys. Lett. B* **668** (2008) 98, doi:10.1016/j.physletb.2008.08.027, arXiv:0804.3664.
- [26] CMS Collaboration, "Search for anomalous $t\bar{t}$ production in the highly-boosted all-hadronic final state", *JHEP* **09** (2012) 029, doi:10.1007/JHEP09(2012)029. [Erratum: doi:10.1007/JHEP03(2014)132].
- [27] ATLAS Collaboration, "A search for $t\bar{t}$ resonances in lepton+jets events with highly boosted top quarks collected in pp collisions at $\sqrt{s} = 7$ TeV with the ATLAS detector", *JHEP* **09** (2012) 041, doi:10.1007/JHEP09(2012)041, arXiv:1207.2409.
- [28] ATLAS Collaboration, "Search for $t\bar{t}$ resonances in the lepton plus jets final state with ATLAS using 4.7 fb^{-1} of pp collisions at $\sqrt{s} = 7$ TeV", *Phys. Rev. D* **88** (2013) 012004, doi:10.1103/PhysRevD.88.012004, arXiv:1305.2756.

- [29] CMS Collaboration, “Search for resonant $t\bar{t}$ production in lepton+jets events in pp collisions at $\sqrt{s} = 7$ TeV”, *JHEP* **12** (2012) 015, doi:10.1007/JHEP12(2012)015.
- [30] CMS Collaboration, “Search for Z' resonances decaying to $t\bar{t}$ in dilepton+jets final states in pp collisions at $\sqrt{s} = 7$ TeV”, *Phys. Rev. D* **87** (2013) 072002, doi:10.1103/PhysRevD.87.072002.
- [31] CMS Collaboration, “Searches for new physics using the $t\bar{t}$ invariant mass distribution in pp collisions at $\sqrt{s}=8$ TeV”, *Phys. Rev. Lett.* **111** (2013) 211804, doi:10.1103/PhysRevLett.111.211804, arXiv:1309.2030. [Erratum *ibid.* **112** (2014) 119903 doi:10.1103/PhysRevLett.112.119903].
- [32] Y. L. Dokshitzer, G. D. Leder, S. Moretti, and B. R. Webber, “Better jet clustering algorithms”, *JHEP* **08** (1997) 001, doi:10.1088/1126-6708/1997/08/001, arXiv:hep-ph/9707323.
- [33] M. Wobisch and T. Wengler, “Hadronization corrections to jet cross sections in deep-inelastic scattering”, (1999). arXiv:hep-ph/9907280.
- [34] D. E. Kaplan, K. Rehermann, M. D. Schwartz, and B. Tweedie, “Top Tagging: A Method for Identifying Boosted Hadronically Decaying Top Quarks”, *Phys. Rev. Lett.* **101** (2008) 142001, doi:10.1103/PhysRevLett.101.142001, arXiv:0806.0848.
- [35] T. Plehn, M. Spannowsky, M. Takeuchi, and D. Zerwas, “Stop Reconstruction with Tagged Tops”, *JHEP* **10** (2010) 078, doi:10.1007/JHEP10(2010)078, arXiv:1006.2833.
- [36] CMS Collaboration, “The CMS experiment at the CERN LHC”, *JINST* **3** (2008) S08004, doi:10.1088/1748-0221/3/08/S08004.
- [37] CMS Collaboration, “Particle-Flow Event Reconstruction in CMS and Performance for Jets, Taus, and E_T^{miss} ”, CMS Physics Analysis Summary CMS-PAS-PFT-09-001, 2009.
- [38] CMS Collaboration, “Commissioning of the Particle-flow Event Reconstruction with the first LHC collisions recorded in the CMS detector”, CMS Physics Analysis Summary CMS-PAS-PFT-10-001, 2010.
- [39] CMS Collaboration, “Description and performance of track and primary-vertex reconstruction with the CMS tracker”, *JINST* **9** (2014) P10009, doi:10.1088/1748-0221/9/10/P10009, arXiv:1405.6569.
- [40] CMS Collaboration, “Performance of Electron Reconstruction and Selection with the CMS Detector in Proton-Proton Collisions at $s = 8$ TeV”, *JINST* **10** (2015) P06005, doi:10.1088/1748-0221/10/06/P06005, arXiv:1502.02701.
- [41] CMS Collaboration, “Energy Calibration and Resolution of the CMS Electromagnetic Calorimeter in pp Collisions at $\sqrt{s} = 7$ TeV”, *JINST* **8** (2013) P09009, doi:10.1088/1748-0221/8/09/P09009, arXiv:1306.2016.
- [42] CMS Collaboration, “Performance of CMS muon reconstruction in pp collision events at $\sqrt{s} = 7$ TeV”, *JINST* **7** (2012) P10002, doi:10.1088/1748-0221/7/10/P10002, arXiv:1206.4071.
- [43] M. Cacciari, G. P. Salam, and G. Soyez, “FastJet user manual”, *Eur. Phys. J. C* **72** (2012) 1896, doi:10.1140/epjc/s10052-012-1896-2, arXiv:1111.6097.

- [44] M. Cacciari, G. P. Salam, and G. Soyez, “The anti- k_t jet clustering algorithm”, *JHEP* **04** (2008) 063, doi:10.1088/1126-6708/2008/04/063, arXiv:0802.1189.
- [45] M. Cacciari, G. P. Salam, and G. Soyez, “The catchment area of jets”, *JHEP* **04** (2008) 005, doi:10.1088/1126-6708/2008/04/005, arXiv:0802.1188.
- [46] CMS Collaboration, “Determination of jet energy calibration and transverse momentum resolution in CMS”, *JINST* **6** (2011) P11002, doi:10.1088/1748-0221/6/11/P11002, arXiv:1107.4277.
- [47] CMS Collaboration, “Identification of b-quark jets with the CMS experiment”, *JINST* **8** (2013) P04013, doi:10.1088/1748-0221/8/04/P04013, arXiv:1211.4462.
- [48] CMS Collaboration, “Jet Performance in pp Collisions at 7 TeV”, CMS Physics Analysis Summary CMS-PAS-JME-10-003, 2010.
- [49] CMS Collaboration, “Missing transverse energy performance of the CMS detector”, *JINST* **6** (2011) P09001, doi:10.1088/1748-0221/6/09/P09001, arXiv:1106.5048.
- [50] CMS Collaboration, “A Cambridge-Aachen (C-A) Based Jet Algorithm For Boosted Top-Jet Tagging”, CMS Physics Analysis Summary CMS-PAS-JME-09-001, 2009.
- [51] CMS Collaboration, “Boosted Top Jet Tagging at CMS”, CMS Physics Analysis Summary CMS-PAS-JME-13-007, 2014.
- [52] J. Thaler and K. Van Tilburg, “Identifying boosted objects with N -subjettiness”, *JHEP* **03** (2011) 015, doi:10.1007/JHEP03(2011)015, arXiv:1011.2268.
- [53] J. Thaler and K. Van Tilburg, “Maximizing boosted top identification by minimizing N -subjettiness”, *JHEP* **02** (2012) 093, doi:10.1007/JHEP02(2012)093, arXiv:1108.2701.
- [54] J. M. Butterworth, A. R. Davison, M. Rubin, and G. P. Salam, “Jet substructure as a new Higgs search channel at the LHC”, *Phys. Rev. Lett.* **100** (2008) 242001, doi:10.1103/PhysRevLett.100.242001, arXiv:0802.2470.
- [55] CMS Collaboration, “Search for vector-like T quarks decaying to top quarks and Higgs bosons in the all-hadronic channel using jet substructure”, *JHEP* **06** (2015) 080, doi:10.1007/JHEP06(2015)080, arXiv:1503.01952.
- [56] CMS Collaboration, “Performance of b tagging at $\sqrt{s} = 8$ TeV in multijet, $t\bar{t}$ and boosted topology events”, CMS Physics Analysis Summary CMS-PAS-BTV-13-001, 2013.
- [57] J. Alwall et al., “MadGraph/MadEvent v4: the new web generation”, *JHEP* **09** (2007) 028, doi:10.1088/1126-6708/2007/09/028, arXiv:0706.2334.
- [58] T. Sjöstrand, S. Mrenna, and P. Skands, “A brief introduction to PYTHIA 8.1”, *Comput. Phys. Commun.* **178** (2008) doi:10.1016/j.cpc.2008.01.036, arXiv:0710.3820.
- [59] P. Nason, “A New method for combining NLO QCD with shower Monte Carlo algorithms”, *JHEP* **11** (2004) 040, doi:10.1088/1126-6708/2004/11/040, arXiv:hep-ph/0409146.

- [60] S. Frixione, P. Nason, and C. Oleari, “Matching NLO QCD computations with parton shower simulations: the POWHEG method”, *JHEP* **11** (2007) 070, doi:10.1088/1126-6708/2007/11/070, arXiv:0709.2092.
- [61] S. Alioli, P. Nason, C. Oleari, and E. Re, “A general framework for implementing NLO calculations in shower Monte Carlo programs: the POWHEG BOX”, *JHEP* **06** (2010) 043, doi:10.1007/JHEP06(2010)043, arXiv:1002.2581.
- [62] J. Alwall et al., “MadGraph 5: going beyond”, *JHEP* **06** (2011) 128, doi:10.1007/JHEP06(2011)128, arXiv:1106.0522.
- [63] T. Sjöstrand, S. Mrenna, and P. Skands, “PYTHIA 6.4 physics and manual”, *JHEP* **05** (2006) 026, doi:10.1088/1126-6708/2006/05/026, arXiv:hep-ph/0603175.
- [64] M. L. Mangano, M. Moretti, F. Piccinini, and M. Treccani, “Matching matrix elements and shower evolution for top-quark production in hadronic collisions”, *JHEP* **01** (2007) 013, doi:10.1088/1126-6708/2007/01/013, arXiv:hep-ph/0611129.
- [65] P. M. Nadolsky et al., “Implications of CTEQ global analysis for collider observables”, *Phys. Rev. D* **78** (2008) 013004, doi:10.1103/PhysRevD.78.013004, arXiv:0802.0007.
- [66] H.-L. Lai et al., “New parton distributions for collider physics”, *Phys. Rev. D* **82** (2010) 074024, doi:10.1103/PhysRevD.82.074024, arXiv:1007.2241.
- [67] R. Field, “Early LHC Underlying Event Data - Findings and Surprises”, (2010). arXiv:1010.3558.
- [68] J. Pumplin et al., “New generation of parton distributions with uncertainties from global QCD analysis”, *JHEP* **07** (2002) 012, doi:10.1088/1126-6708/2002/07/012, arXiv:hep-ph/0201195.
- [69] J. Gao et al., “Next-to-leading order QCD corrections to a heavy resonance production and decay into top quark pair at the LHC”, *Phys. Rev. D* **82** (2010) 014020, doi:10.1103/PhysRevD.82.014020, arXiv:1004.0876.
- [70] N. Kidonakis, “NNLL threshold resummation for top-pair and single-top production”, *Phys. Part. Nucl.* **45** (2014) 714, doi:10.1134/S1063779614040091, arXiv:1210.7813.
- [71] R. Gavin, Y. Li, F. Petriello, and S. Quackenbush, “FEWZ 2.0: A code for hadronic Z production at next-to-next-to-leading order”, *Comput. Phys. Commun.* **182** (2011) 2388, doi:10.1016/j.cpc.2011.06.008, arXiv:1011.3540.
- [72] R. Gavin, Y. Li, F. Petriello, and S. Quackenbush, “W Physics at the LHC with FEWZ 2.1”, *Comput. Phys. Commun.* **184** (2013) 208, doi:10.1016/j.cpc.2012.09.005, arXiv:1201.5896.
- [73] Y. Li and F. Petriello, “Combining QCD and electroweak corrections to dilepton production in FEWZ”, *Phys. Rev. D* **86** (2012) 094034, doi:10.1103/PhysRevD.86.094034, arXiv:1208.5967.
- [74] J. M. Campbell, R. K. Ellis, and K. Williams, “Vector boson pair production at the LHC”, *JHEP* **07** (2011) 018, doi:10.1007/JHEP07(2011)018, arXiv:1105.0020.

- [75] M. Czakon, P. Fiedler, and A. Mitov, “Total Top-Quark Pair-Production Cross Section at Hadron Colliders Through $O(\alpha_s^4)$ ”, *Phys. Rev. Lett.* **110** (2013) 252004, doi:10.1103/PhysRevLett.110.252004, arXiv:1303.6254.
- [76] GEANT4 Collaboration, “GEANT4—a simulation toolkit”, *Nucl. Instrum. Meth. A* **506** (2003) 250, doi:10.1016/S0168-9002(03)01368-8.
- [77] CMS Collaboration, “Measurement of the differential cross section for top quark pair production in pp collisions at $\sqrt{s} = 8$ TeV”, *Eur. Phys. J.* **C75** (2015) 542, doi:10.1140/epjc/s10052-015-3709-x, arXiv:1505.04480.
- [78] CMS Collaboration, “Differential cross section measurements for the production of a W boson in association with jets in proton-proton collisions at $\sqrt{s} = 7$ TeV”, *Phys. Lett. B* **741** (2015) 12, doi:10.1016/j.physletb.2014.12.003, arXiv:1406.7533.
- [79] CMS Collaboration, “Measurement of the production cross section for a W boson and two b jets in pp collisions at $\sqrt{s}=7$ TeV”, *Phys. Lett. B* **735** (2014) 204, doi:10.1016/j.physletb.2014.06.041, arXiv:1312.6608.
- [80] CMS Collaboration, “Observation of the associated production of a single top quark and a W boson in pp collisions at $\sqrt{s} = 8$ TeV”, *Phys. Rev. Lett.* **112** (2014) 231802, doi:10.1103/PhysRevLett.112.231802, arXiv:1401.2942.
- [81] CMS Collaboration, “Measurement of W^+W^- and ZZ production cross sections in pp collisions at $\sqrt{s} = 8$ TeV”, *Phys. Lett. B* **721** (2013) 190, doi:10.1016/j.physletb.2013.03.027, arXiv:1301.4698.
- [82] CMS Collaboration, “Measurement of WZ and ZZ production in pp collisions at $\sqrt{s} = 8$ TeV in final states with b-tagged jets”, *Eur. Phys. J. C* **74** (2014) 2973, doi:10.1140/epjc/s10052-014-2973-5, arXiv:1403.3047.
- [83] CMS Collaboration, “CMS Luminosity Based on Pixel Cluster Counting – Summer 2013 Update”, CMS Physics Analysis Summary CMS-PAS-LUM-13-001, 2013.
- [84] A. O’Hagan and J. J. Forster, “Kendall’s Advanced Theory of Statistics. Vol. 2B: Bayesian Inference”. Arnold, London, 2004.
- [85] J. Ott. <http://www.theta-framework.org>.

A Uncertainty on the background estimate in all-hadronic channel

As mentioned in Section 5, in the high-mass all-hadronic analysis, the mistag rate r is parameterized as a function of the jet p_T , the N -subjettiness ratio τ_{32} , and the b-tagging discriminant β , of the jet “ a ”. In the low-mass analysis, the mistag rate is parameterized as a function of jet p_T and β only, but the procedure is otherwise identical.

Taking the high-mass analysis as an example, the non-top-quark multijet background arising from events with mistagged light jets is estimated by dividing the data into bins along four dimensions: jet p_T , τ_{32} , β , and the variable of interest α (in this case $M_{\bar{t}t}$, although the procedure is applicable to any other variable).

The expected background yield for this 4-dimensional bin is obtained by multiplying the events in this bin before the application of t tagging, $N(M_{\bar{t}t}, p_T, \tau_{32}, \beta) = N_{\alpha,i,j,k}$, by the mistag rate

$r(p_T, \tau_{32}, \beta) = r_{i,j,k}$. Summing all the predictions along indices i, j , and k then yields the total prediction for the bin α :

$$N_\alpha = \sum_{a=1}^{N_{\text{jets}}} N_{\alpha,i,j,k} r_{i,j,k},$$

where N_{jets} is the number of jets in the event. The four-dimensional parameterization properly accounts for correlated and uncorrelated statistical uncertainties. The uncertainty in each bin of the predicted mistagged distribution $\sigma(m_\alpha)$ has two parts: one arises from the misidentification probability ($\sigma(r_{i,j,k})$), and the other from the number of jets in the ensemble ($\sqrt{N_{\alpha,i,j,k}}$):

$$\sigma(m_\alpha) = \sqrt{\sum_{a=1}^{N_{\text{jets}}} \left((N_{\alpha,i,j,k} \sigma(r_{i,j,k}))^2 + (\sqrt{N_{\alpha,i,j,k}} r_{i,j,k})^2 \right)},$$

The first term accounts for all uncertainties in the i, j, k -th bin of the mistag probability. The second term accounts for statistical uncertainties in the jet ensemble. Both of these terms are individually added linearly since they are fully correlated within each bin. The two pieces are added in quadrature since they are fully uncorrelated.

B The CMS Collaboration

Yerevan Physics Institute, Yerevan, Armenia

V. Khachatryan, A.M. Sirunyan, A. Tumasyan

Institut für Hochenergiephysik der OeAW, Wien, Austria

W. Adam, E. Asilar, T. Bergauer, J. Brandstetter, E. Brondolin, M. Dragicevic, J. Erö, M. Flechl, M. Friedl, R. Frühwirth¹, V.M. Ghete, C. Hartl, N. Hörmann, J. Hrubec, M. Jeitler¹, V. Knünz, A. König, M. Krammer¹, I. Krätschmer, D. Liko, T. Matsushita, I. Mikulec, D. Rabady², B. Rahbaran, H. Rohringer, J. Schieck¹, R. Schöfbeck, J. Strauss, W. Treberer-Treberspurg, W. Waltenberger, C.-E. Wulz¹

National Centre for Particle and High Energy Physics, Minsk, Belarus

V. Mossolov, N. Shumeiko, J. Suarez Gonzalez

Universiteit Antwerpen, Antwerpen, Belgium

S. Alderweireldt, T. Cornelis, E.A. De Wolf, X. Janssen, A. Knutsson, J. Lauwers, S. Luyckx, S. Ochesanu, R. Rougny, M. Van De Klundert, H. Van Haevermaet, P. Van Mechelen, N. Van Remortel, A. Van Spilbeek

Vrije Universiteit Brussel, Brussel, Belgium

S. Abu Zeid, F. Blekman, J. D'Hondt, N. Daci, I. De Bruyn, K. Deroover, N. Heracleous, J. Keaveney, S. Lowette, L. Moreels, A. Olbrechts, Q. Python, D. Strom, S. Tavernier, W. Van Doninck, P. Van Mulders, G.P. Van Onsem, I. Van Parijs

Université Libre de Bruxelles, Bruxelles, Belgium

P. Barria, C. Caillol, B. Clerboux, G. De Lentdecker, H. Delannoy, D. Dobur, G. Fasanella, L. Favart, A.P.R. Gay, A. Grebenyuk, T. Lenzi, A. Léonard, T. Maerschalk, A. Mohammadi, L. Perniè, A. Randle-conde, T. Reis, T. Seva, L. Thomas, C. Vander Velde, P. Vanlaer, J. Wang, R. Yonamine, F. Zenoni, F. Zhang³

Ghent University, Ghent, Belgium

K. Beernaert, L. Benucci, A. Cimmino, S. Crucy, A. Fagot, G. Garcia, M. Gul, J. Mccartin, A.A. Ocampo Rios, D. Poyraz, D. Ryckbosch, S. Salva Diblen, M. Sigamani, N. Strobbe, M. Tytgat, W. Van Driessche, E. Yazgan, N. Zaganidis

Université Catholique de Louvain, Louvain-la-Neuve, Belgium

S. Basesmez, C. Beluffi⁴, O. Bondu, G. Bruno, R. Castello, A. Caudron, L. Ceard, G.G. Da Silva, C. Delaere, D. Favart, L. Forthomme, A. Giammanco⁵, J. Hollar, A. Jafari, P. Jez, M. Komm, V. Lemaître, A. Mertens, C. Nuttens, L. Perrini, A. Pin, K. Piotrkowski, A. Popov⁶, L. Quertenmont, M. Selvaggi, M. Vidal Marono

Université de Mons, Mons, Belgium

N. Belyi, T. Caebegs, G.H. Hammad

Centro Brasileiro de Pesquisas Físicas, Rio de Janeiro, Brazil

W.L. Aldá Júnior, G.A. Alves, L. Brito, M. Correa Martins Junior, T. Dos Reis Martins, C. Hensel, C. Mora Herrera, A. Moraes, M.E. Pol, P. Rebello Teles

Universidade do Estado do Rio de Janeiro, Rio de Janeiro, Brazil

E. Belchior Batista Das Chagas, W. Carvalho, J. Chinellato⁷, A. Custódio, E.M. Da Costa, D. De Jesus Damiao, C. De Oliveira Martins, S. Fonseca De Souza, L.M. Huertas Guativa, H. Malbouisson, D. Matos Figueiredo, L. Mundim, H. Nogima, W.L. Prado Da Silva, A. Santoro, A. Sznajder, E.J. Tonelli Manganote⁷, A. Vilela Pereira

Universidade Estadual Paulista ^a, Universidade Federal do ABC ^b, São Paulo, Brazil

S. Ahuja^a, C.A. Bernardes^b, A. De Souza Santos^b, S. Dogra^a, T.R. Fernandez Perez Tomei^a, E.M. Gregores^b, P.G. Mercadante^b, C.S. Moon^{a,8}, S.F. Novaes^a, Sandra S. Padula^a, D. Romero Abad, J.C. Ruiz Vargas

Institute for Nuclear Research and Nuclear Energy, Sofia, Bulgaria

A. Aleksandrov, V. Genchev², R. Hadjiiska, P. Iaydjiev, A. Marinov, S. Piperov, M. Rodozov, S. Stoykova, G. Sultanov, M. Vutova

University of Sofia, Sofia, Bulgaria

A. Dimitrov, I. Glushkov, L. Litov, B. Pavlov, P. Petkov

Institute of High Energy Physics, Beijing, China

M. Ahmad, J.G. Bian, G.M. Chen, H.S. Chen, M. Chen, T. Cheng, R. Du, C.H. Jiang, R. Plestina⁹, F. Romeo, S.M. Shaheen, J. Tao, C. Wang, Z. Wang, H. Zhang

State Key Laboratory of Nuclear Physics and Technology, Peking University, Beijing, China

C. Asawatrangkuldee, Y. Ban, Q. Li, S. Liu, Y. Mao, S.J. Qian, D. Wang, Z. Xu, W. Zou

Universidad de Los Andes, Bogota, Colombia

C. Avila, A. Cabrera, L.F. Chaparro Sierra, C. Florez, J.P. Gomez, B. Gomez Moreno, J.C. Sanabria

University of Split, Faculty of Electrical Engineering, Mechanical Engineering and Naval Architecture, Split, Croatia

N. Godinovic, D. Lelas, D. Polic, I. Puljak

University of Split, Faculty of Science, Split, Croatia

Z. Antunovic, M. Kovac

Institute Rudjer Boskovic, Zagreb, Croatia

V. Brigljevic, K. Kadija, J. Luetic, L. Sudic

University of Cyprus, Nicosia, Cyprus

A. Attikis, G. Mavromanolakis, J. Mousa, C. Nicolaou, F. Ptochos, P.A. Razis, H. Rykaczewski

Charles University, Prague, Czech Republic

M. Bodlak, M. Finger¹⁰, M. Finger Jr.¹⁰

Academy of Scientific Research and Technology of the Arab Republic of Egypt, Egyptian Network of High Energy Physics, Cairo, Egypt

A. Ali^{11,12}, R. Aly¹³, S. Aly¹³, Y. Assran¹⁴, A. Ellithi Kamel¹⁵, A. Lotfy¹⁶, M.A. Mahmoud¹⁶, R. Masod¹¹, A. Radi^{12,11}

National Institute of Chemical Physics and Biophysics, Tallinn, Estonia

B. Calpas, M. Kadastik, M. Murumaa, M. Raidal, A. Tiko, C. Veelken

Department of Physics, University of Helsinki, Helsinki, Finland

P. Eerola, M. Voutilainen

Helsinki Institute of Physics, Helsinki, Finland

J. Härkönen, V. Karimäki, R. Kinnunen, T. Lampén, K. Lassila-Perini, S. Lehti, T. Lindén, P. Luukka, T. Mäenpää, J. Pekkanen, T. Peltola, E. Tuominen, J. Tuominiemi, E. Tuovinen, L. Wendland

Lappeenranta University of Technology, Lappeenranta, Finland

J. Talvitie, T. Tuuva

DSM/IRFU, CEA/Saclay, Gif-sur-Yvette, France

M. Besancon, F. Couderc, M. Dejardin, D. Denegri, B. Fabbro, J.L. Faure, C. Favaro, F. Ferri, S. Ganjour, A. Givernaud, P. Gras, G. Hamel de Monchenault, P. Jarry, E. Locci, M. Machet, J. Malcles, J. Rander, A. Rosowsky, M. Titov, A. Zghiche

Laboratoire Leprince-Ringuet, Ecole Polytechnique, IN2P3-CNRS, Palaiseau, France

S. Baffioni, F. Beaudette, P. Busson, L. Cadamuro, E. Chapon, C. Charlot, T. Dahms, O. Davignon, N. Filipovic, A. Florent, R. Granier de Cassagnac, S. Lisniak, L. Mastrolorenzo, P. Miné, I.N. Naranjo, M. Nguyen, C. Ochando, G. Ortona, P. Paganini, S. Regnard, R. Salerno, J.B. Sauvan, Y. Sirois, T. Strebler, Y. Yilmaz, A. Zabi

Institut Pluridisciplinaire Hubert Curien, Université de Strasbourg, Université de Haute Alsace Mulhouse, CNRS/IN2P3, Strasbourg, France

J.-L. Agram¹⁷, J. Andrea, A. Aubin, D. Bloch, J.-M. Brom, M. Buttignol, E.C. Chabert, N. Chanon, C. Collard, E. Conte¹⁷, J.-C. Fontaine¹⁷, D. Gelé, U. Goerlach, C. Goetzmann, A.-C. Le Bihan, J.A. Merlin², K. Skovpen, P. Van Hove

Centre de Calcul de l'Institut National de Physique Nucleaire et de Physique des Particules, CNRS/IN2P3, Villeurbanne, France

S. Gadrat

Université de Lyon, Université Claude Bernard Lyon 1, CNRS-IN2P3, Institut de Physique Nucléaire de Lyon, Villeurbanne, France

S. Beauceron, C. Bernet⁹, G. Boudoul, E. Bouvier, S. Brochet, C.A. Carrillo Montoya, J. Chasserat, R. Chierici, D. Contardo, B. Courbon, P. Depasse, H. El Mamouni, J. Fan, J. Fay, S. Gascon, M. Gouzevitch, B. Ille, I.B. Laktineh, M. Lethuillier, L. Mirabito, A.L. Pequegnot, S. Perries, J.D. Ruiz Alvarez, D. Sabes, L. Sgandurra, V. Sordini, M. Vander Donckt, P. Verdier, S. Viret, H. Xiao

Institute of High Energy Physics and Informatization, Tbilisi State University, Tbilisi, Georgia

Z. Tsamalaidze¹⁰

RWTH Aachen University, I. Physikalisches Institut, Aachen, Germany

C. Autermann, S. Beranek, M. Edelhoff, L. Feld, A. Heister, M.K. Kiesel, K. Klein, M. Lipinski, A. Ostapchuk, M. Preuten, F. Raupach, J. Sammet, S. Schael, J.F. Schulte, T. Verlage, H. Weber, B. Wittmer, V. Zhukov⁶

RWTH Aachen University, III. Physikalisches Institut A, Aachen, Germany

M. Ata, M. Brodski, E. Dietz-Laursonn, D. Duchardt, M. Endres, M. Erdmann, S. Erdweg, T. Esch, R. Fischer, A. Güth, T. Hebbeker, C. Heidemann, K. Hoepfner, D. Klingebiel, S. Knutzen, P. Kreuzer, M. Merschmeyer, A. Meyer, P. Millet, M. Olschewski, K. Padeken, P. Papacz, T. Pook, M. Radziej, H. Reithler, M. Rieger, F. Scheuch, L. Sonnenschein, D. Teyssier, S. Thüer

RWTH Aachen University, III. Physikalisches Institut B, Aachen, Germany

V. Cherepanov, Y. Erdogan, G. Flügge, H. Geenen, M. Geisler, W. Haj Ahmad, F. Hoehle, B. Kargoll, T. Kress, Y. Kuessel, A. Künsken, J. Lingemann², A. Nehr Korn, A. Nowack, I.M. Nugent, C. Pistone, O. Pooth, A. Stahl

Deutsches Elektronen-Synchrotron, Hamburg, Germany

M. Aldaya Martin, I. Asin, N. Bartosik, O. Behnke, U. Behrens, A.J. Bell, K. Borras, A. Burgmeier, A. Cakir, L. Calligaris, A. Campbell, S. Choudhury, F. Costanza, C. Diez Pardos, G. Dolinska, S. Dooling, T. Dorland, G. Eckerlin, D. Eckstein, T. Eichhorn, G. Flucke,

E. Gallo, J. Garay Garcia, A. Geiser, A. Gizhko, P. Gunnellini, J. Hauk, M. Hempel¹⁸, H. Jung, A. Kalogeropoulos, O. Karacheban¹⁸, M. Kasemann, P. Katsas, J. Kieseler, C. Kleinwort, I. Korol, W. Lange, J. Leonard, K. Lipka, A. Lobanov, W. Lohmann¹⁸, R. Mankel, I. Marfin¹⁸, I.-A. Melzer-Pellmann, A.B. Meyer, G. Mittag, J. Mnich, A. Mussgiller, S. Naumann-Emme, A. Nayak, E. Ntomari, H. Perrey, D. Pitzl, R. Placakyte, A. Raspereza, P.M. Ribeiro Cipriano, B. Roland, M.Ö. Sahin, J. Salfeld-Nebgen, P. Saxena, T. Schoerner-Sadenius, M. Schröder, C. Seitz, S. Spannagel, K.D. Trippkewitz, C. Wissing

University of Hamburg, Hamburg, Germany

V. Blobel, M. Centis Vignali, A.R. Draeger, J. Erfle, E. Garutti, K. Goebel, D. Gonzalez, M. Görner, J. Haller, M. Hoffmann, R.S. Höing, A. Junkes, R. Klanner, R. Kogler, T. Lapsien, T. Lenz, I. Marchesini, D. Marconi, D. Nowatschin, J. Ott, F. Pantaleo², T. Peiffer, A. Perieanu, N. Pietsch, J. Poehlsen, D. Rathjens, C. Sander, H. Schettler, P. Schleper, E. Schlieckau, A. Schmidt, J. Schwandt, M. Seidel, V. Sola, H. Stadie, G. Steinbrück, H. Tholen, D. Troendle, E. Usai, L. Vaneldereren, A. Vanhoefer

Institut für Experimentelle Kernphysik, Karlsruhe, Germany

M. Akbiyik, C. Barth, C. Baus, J. Berger, C. Böser, E. Butz, T. Chwalek, F. Colombo, W. De Boer, A. Descroix, A. Dierlamm, M. Feindt, F. Frensch, M. Giffels, A. Gilbert, F. Hartmann², U. Husemann, F. Kassel², I. Katkov⁶, A. Kornmayer², P. Lobelle Pardo, M.U. Mozer, T. Müller, Th. Müller, M. Plagge, G. Quast, K. Rabbertz, S. Röcker, F. Roscher, H.J. Simonis, F.M. Stober, R. Ulrich, J. Wagner-Kuhr, S. Wayand, T. Weiler, C. Wöhrmann, R. Wolf

Institute of Nuclear and Particle Physics (INPP), NCSR Demokritos, Aghia Paraskevi, Greece

G. Anagnostou, G. Daskalakis, T. Gerasis, V.A. Giakoumopoulou, A. Kyriakis, D. Loukas, A. Markou, A. Psallidas, I. Topsis-Giotis

University of Athens, Athens, Greece

A. Agapitos, S. Kesisoglou, A. Panagiotou, N. Saoulidou, E. Tziaferi

University of Ioánnina, Ioánnina, Greece

I. Evangelou, G. Flouris, C. Foudas, P. Kokkas, N. Loukas, N. Manthos, I. Papadopoulos, E. Paradas, J. Strologas

Wigner Research Centre for Physics, Budapest, Hungary

G. Bencze, C. Hajdu, A. Hazi, P. Hidas, D. Horvath¹⁹, F. Sikler, V. Veszpremi, G. Vesztergombi²⁰, A.J. Zsigmond

Institute of Nuclear Research ATOMKI, Debrecen, Hungary

N. Beni, S. Czellar, J. Karancsi²¹, J. Molnar, Z. Szillasi

University of Debrecen, Debrecen, Hungary

M. Bartók²², A. Makovec, P. Raics, Z.L. Trocsanyi, B. Ujvari

National Institute of Science Education and Research, Bhubaneswar, India

P. Mal, K. Mandal, N. Sahoo, S.K. Swain

Panjab University, Chandigarh, India

S. Bansal, S.B. Beri, V. Bhatnagar, R. Chawla, R. Gupta, U. Bhawandeep, A.K. Kalsi, A. Kaur, M. Kaur, R. Kumar, A. Mehta, M. Mittal, N. Nishu, J.B. Singh, G. Walia

University of Delhi, Delhi, India

Ashok Kumar, Arun Kumar, A. Bhardwaj, B.C. Choudhary, R.B. Garg, A. Kumar, S. Malhotra, M. Naimuddin, K. Ranjan, R. Sharma, V. Sharma

Saha Institute of Nuclear Physics, Kolkata, India

S. Banerjee, S. Bhattacharya, K. Chatterjee, S. Dey, S. Dutta, Sa. Jain, Sh. Jain, R. Khurana, N. Majumdar, A. Modak, K. Mondal, S. Mukherjee, S. Mukhopadhyay, A. Roy, D. Roy, S. Roy Chowdhury, S. Sarkar, M. Sharan

Bhabha Atomic Research Centre, Mumbai, India

A. Abdulsalam, R. Chudasama, D. Dutta, V. Jha, V. Kumar, A.K. Mohanty², L.M. Pant, P. Shukla, A. Topkar

Tata Institute of Fundamental Research, Mumbai, India

T. Aziz, S. Banerjee, S. Bhowmik²³, R.M. Chatterjee, R.K. Dewanjee, S. Dugad, S. Ganguly, S. Ghosh, M. Guchait, A. Gurtu²⁴, G. Kole, S. Kumar, B. Mahakud, M. Maity²³, G. Majumder, K. Mazumdar, S. Mitra, G.B. Mohanty, B. Parida, T. Sarkar²³, K. Sudhakar, N. Sur, B. Sutar, N. Wickramage²⁵

Indian Institute of Science Education and Research (IISER), Pune, India

S. Sharma

Institute for Research in Fundamental Sciences (IPM), Tehran, Iran

H. Bakhshiansohi, H. Behnamian, S.M. Etesami²⁶, A. Fahim²⁷, R. Goldouzian, M. Khakzad, M. Mohammadi Najafabadi, M. Naseri, S. Paktinat Mehdiabadi, F. Rezaei Hosseinabadi, B. Safarzadeh²⁸, M. Zeinali

University College Dublin, Dublin, Ireland

M. Felcini, M. Grunewald

INFN Sezione di Bari ^a, Università di Bari ^b, Politecnico di Bari ^c, Bari, Italy

M. Abbrescia^{a,b}, C. Calabria^{a,b}, C. Caputo^{a,b}, S.S. Chhibra^{a,b}, A. Colaleo^a, D. Creanza^{a,c}, L. Cristella^{a,b}, N. De Filippis^{a,c}, M. De Palma^{a,b}, L. Fiore^a, G. Iaselli^{a,c}, G. Maggi^{a,c}, M. Maggi^a, G. Miniello^{a,b}, S. My^{a,c}, S. Nuzzo^{a,b}, A. Pompili^{a,b}, G. Pugliese^{a,c}, R. Radogna^{a,b}, A. Ranieri^a, G. Selvaggi^{a,b}, A. Sharma^a, L. Silvestris^{a,2}, R. Venditti^{a,b}, P. Verwilligen^a

INFN Sezione di Bologna ^a, Università di Bologna ^b, Bologna, Italy

G. Abbiendi^a, C. Battilana², A.C. Benvenuti^a, D. Bonacorsi^{a,b}, S. Braibant-Giacomelli^{a,b}, L. Brigliadori^{a,b}, R. Campanini^{a,b}, P. Capiluppi^{a,b}, A. Castro^{a,b}, F.R. Cavallo^a, G. Codispoti^{a,b}, M. Cuffiani^{a,b}, G.M. Dallavalle^a, F. Fabbri^a, A. Fanfani^{a,b}, D. Fasanella^{a,b}, P. Giacomelli^a, C. Grandi^a, L. Guiducci^{a,b}, S. Marcellini^a, G. Masetti^a, A. Montanari^a, F.L. Navarria^{a,b}, A. Perrotta^a, A.M. Rossi^{a,b}, T. Rovelli^{a,b}, G.P. Siroli^{a,b}, N. Tosi^{a,b}, R. Travaglini^{a,b}

INFN Sezione di Catania ^a, Università di Catania ^b, CSFNSM ^c, Catania, Italy

G. Cappello^a, M. Chiorboli^{a,b}, S. Costa^{a,b}, F. Giordano^a, R. Potenza^{a,b}, A. Tricomi^{a,b}, C. Tuve^{a,b}

INFN Sezione di Firenze ^a, Università di Firenze ^b, Firenze, Italy

G. Barbagli^a, V. Ciulli^{a,b}, C. Civinini^a, R. D'Alessandro^{a,b}, E. Focardi^{a,b}, S. Gonzi^{a,b}, V. Gori^{a,b}, P. Lenzi^{a,b}, M. Meschini^a, S. Paoletti^a, G. Sguazzoni^a, A. Tropiano^{a,b}, L. Viliani^{a,b}

INFN Laboratori Nazionali di Frascati, Frascati, Italy

L. Benussi, S. Bianco, F. Fabbri, D. Piccolo

INFN Sezione di Genova ^a, Università di Genova ^b, Genova, Italy

V. Calvelli^{a,b}, F. Ferro^a, M. Lo Vetere^{a,b}, E. Robutti^a, S. Tosi^{a,b}

INFN Sezione di Milano-Bicocca ^a, Università di Milano-Bicocca ^b, Milano, Italy

M.E. Dinardo^{a,b}, S. Fiorendi^{a,b}, S. Gennai^a, R. Gerosa^{a,b}, A. Ghezzi^{a,b}, P. Govoni^{a,b}, S. Malvezzi^a,

R.A. Manzoni^{a,b}, B. Marzocchi^{a,b,2}, D. Menasce^a, L. Moroni^a, M. Paganoni^{a,b}, D. Pedrini^a, S. Ragazzi^{a,b}, N. Redaelli^a, T. Tabarelli de Fatis^{a,b}

INFN Sezione di Napoli^a, Università di Napoli 'Federico II'^b, Napoli, Italy, Università della Basilicata^c, Potenza, Italy, Università G. Marconi^d, Roma, Italy

S. Buontempo^a, N. Cavallo^{a,c}, S. Di Guida^{a,d,2}, M. Esposito^{a,b}, F. Fabozzi^{a,c}, A.O.M. Iorio^{a,b}, G. Lanza^a, L. Lista^a, S. Meola^{a,d,2}, M. Merola^a, P. Paolucci^{a,2}, C. Sciacca^{a,b}, F. Thyssen

INFN Sezione di Padova^a, Università di Padova^b, Padova, Italy, Università di Trento^c, Trento, Italy

P. Azzi^{a,2}, N. Bacchetta^a, D. Bisello^{a,b}, A. Branca^{a,b}, R. Carlin^{a,b}, A. Carvalho Antunes De Oliveira^{a,b}, P. Checchia^a, M. Dall'Osso^{a,b,2}, T. Dorigo^a, F. Gasparini^{a,b}, U. Gasparini^{a,b}, F. Gonella^a, A. Gozzelino^a, K. Kanishchev^{a,c}, S. Lacaprara^a, M. Margoni^{a,b}, A.T. Meneguzzo^{a,b}, F. Montecassiano^a, J. Pazzini^{a,b}, N. Pozzobon^{a,b}, P. Ronchese^{a,b}, F. Simonetto^{a,b}, E. Torassa^a, M. Tosi^{a,b}, M. Zanetti, P. Zotto^{a,b}, A. Zucchetta^{a,b,2}

INFN Sezione di Pavia^a, Università di Pavia^b, Pavia, Italy

A. Braghieri^a, M. Gabusi^{a,b}, A. Magnani^a, S.P. Ratti^{a,b}, V. Re^a, C. Riccardi^{a,b}, P. Salvini^a, I. Vai^a, P. Vitulo^{a,b}

INFN Sezione di Perugia^a, Università di Perugia^b, Perugia, Italy

L. Alunni Solestizi^{a,b}, M. Biasini^{a,b}, G.M. Bilei^a, D. Ciangottini^{a,b,2}, L. Fanò^{a,b}, P. Lariccia^{a,b}, G. Mantovani^{a,b}, M. Menichelli^a, A. Saha^a, A. Santocchia^{a,b}, A. Spiezia^{a,b}

INFN Sezione di Pisa^a, Università di Pisa^b, Scuola Normale Superiore di Pisa^c, Pisa, Italy

K. Androsov^{a,29}, P. Azzurri^a, G. Bagliesi^a, J. Bernardini^a, T. Boccali^a, G. Broccolo^{a,c}, R. Castaldi^a, M.A. Ciocci^{a,29}, R. Dell'Orso^a, S. Donato^{a,c,2}, G. Fedi, L. Foà^{a,c†}, A. Giassi^a, M.T. Grippo^{a,29}, F. Ligabue^{a,c}, T. Lomtadze^a, L. Martini^{a,b}, A. Messineo^{a,b}, F. Palla^a, A. Rizzi^{a,b}, A. Savoy-Navarro^{a,30}, A.T. Serban^a, P. Spagnolo^a, P. Squillacioti^{a,29}, R. Tenchini^a, G. Tonelli^{a,b}, A. Venturi^a, P.G. Verdini^a

INFN Sezione di Roma^a, Università di Roma^b, Roma, Italy

L. Barone^{a,b}, F. Cavallari^a, G. D'imperio^{a,b,2}, D. Del Re^{a,b}, M. Diemoz^a, S. Gelli^{a,b}, C. Jorda^a, E. Longo^{a,b}, F. Margaroli^{a,b}, P. Meridiani^a, F. Micheli^{a,b}, G. Organtini^{a,b}, R. Paramatti^a, F. Preiato^{a,b}, S. Rahatlou^{a,b}, C. Rovelli^a, F. Santanastasio^{a,b}, P. Traczyk^{a,b,2}

INFN Sezione di Torino^a, Università di Torino^b, Torino, Italy, Università del Piemonte Orientale^c, Novara, Italy

N. Amapane^{a,b}, R. Arcidiacono^{a,c}, S. Argiro^{a,b}, M. Arneodo^{a,c}, R. Bellan^{a,b}, C. Biino^a, N. Cartiglia^a, M. Costa^{a,b}, R. Covarelli^{a,b}, A. Degano^{a,b}, G. Dellacasa^a, N. Demaria^a, L. Finco^{a,b,2}, C. Mariotti^a, S. Maselli^a, G. Mazza^a, E. Migliore^{a,b}, V. Monaco^{a,b}, E. Monteil^{a,b}, M. Musich^a, M.M. Obertino^{a,b}, L. Pacher^{a,b}, N. Pastrone^a, M. Pelliccioni^a, G.L. Pinna Angioni^{a,b}, F. Ravera^{a,b}, A. Romero^{a,b}, M. Ruspa^{a,c}, R. Sacchi^{a,b}, A. Solano^{a,b}, A. Staiano^a

INFN Sezione di Trieste^a, Università di Trieste^b, Trieste, Italy

S. Belforte^a, V. Candelise^{a,b,2}, M. Casarsa^a, F. Cossutti^a, G. Della Ricca^{a,b}, B. Gobbo^a, C. La Licata^{a,b}, M. Marone^{a,b}, A. Schizzi^{a,b}, T. Umer^{a,b}, A. Zanetti^a

Kangwon National University, Chunchon, Korea

S. Chang, A. Kropivnitskaya, S.K. Nam

Kyungpook National University, Daegu, Korea

D.H. Kim, G.N. Kim, M.S. Kim, D.J. Kong, S. Lee, Y.D. Oh, A. Sakharov, D.C. Son

Chonbuk National University, Jeonju, Korea

H. Kim, T.J. Kim, M.S. Ryu

Chonnam National University, Institute for Universe and Elementary Particles, Kwangju, Korea

S. Song

Korea University, Seoul, Korea

S. Choi, Y. Go, D. Gyun, B. Hong, M. Jo, H. Kim, Y. Kim, B. Lee, K. Lee, K.S. Lee, S. Lee, S.K. Park, Y. Roh

Seoul National University, Seoul, Korea

H.D. Yoo

University of Seoul, Seoul, Korea

M. Choi, J.H. Kim, J.S.H. Lee, I.C. Park, G. Ryu

Sungkyunkwan University, Suwon, Korea

Y. Choi, Y.K. Choi, J. Goh, D. Kim, E. Kwon, J. Lee, I. Yu

Vilnius University, Vilnius, Lithuania

A. Juodagalvis, J. Vaitkus

National Centre for Particle Physics, Universiti Malaya, Kuala Lumpur, Malaysia

Z.A. Ibrahim, J.R. Komaragiri, M.A.B. Md Ali³¹, F. Mohamad Idris, W.A.T. Wan Abdullah

Centro de Investigacion y de Estudios Avanzados del IPN, Mexico City, Mexico

E. Casimiro Linares, H. Castilla-Valdez, E. De La Cruz-Burelo, I. Heredia-de La Cruz³², A. Hernandez-Almada, R. Lopez-Fernandez, G. Ramirez Sanchez, A. Sanchez-Hernandez

Universidad Iberoamericana, Mexico City, Mexico

S. Carrillo Moreno, F. Vazquez Valencia

Benemerita Universidad Autonoma de Puebla, Puebla, Mexico

S. Carpinteyro, I. Pedraza, H.A. Salazar Ibarguen

Universidad Autónoma de San Luis Potosí, San Luis Potosí, Mexico

A. Morelos Pineda

University of Auckland, Auckland, New Zealand

D. Krofcheck

University of Canterbury, Christchurch, New Zealand

P.H. Butler, S. Reucroft

National Centre for Physics, Quaid-I-Azam University, Islamabad, Pakistan

A. Ahmad, M. Ahmad, Q. Hassan, H.R. Hoorani, W.A. Khan, T. Khurshid, M. Shoaib

National Centre for Nuclear Research, Swierk, Poland

H. Bialkowska, M. Bluj, B. Boimska, T. Frueboes, M. Górski, M. Kazana, K. Nawrocki, K. Romanowska-Rybinska, M. Szleper, P. Zalewski

Institute of Experimental Physics, Faculty of Physics, University of Warsaw, Warsaw, Poland

G. Brona, K. Bunkowski, K. Doroba, A. Kalinowski, M. Konecki, J. Krolikowski, M. Misiura, M. Olszewski, M. Walczak

Laboratório de Instrumentação e Física Experimental de Partículas, Lisboa, Portugal

P. Bargassa, C. Beirão Da Cruz E Silva, A. Di Francesco, P. Faccioli, P.G. Ferreira Parracho,

M. Gallinaro, L. Lloret Iglesias, F. Nguyen, J. Rodrigues Antunes, J. Seixas, O. Toldaiev, D. Vadrucio, J. Varela, P. Vischia

Joint Institute for Nuclear Research, Dubna, Russia

S. Afanasiev, P. Bunin, M. Gavrilenko, I. Golutvin, I. Gorbunov, A. Kamenev, V. Karjavin, V. Konoplyanikov, A. Lanev, A. Malakhov, V. Matveev³³, P. Moisenz, V. Palichik, V. Perelygin, S. Shmatov, S. Shulha, N. Skatchkov, V. Smirnov, T. Toriashvili³⁴, A. Zarubin

Petersburg Nuclear Physics Institute, Gatchina (St. Petersburg), Russia

V. Golovtsov, Y. Ivanov, V. Kim³⁵, E. Kuznetsova, P. Levchenko, V. Murzin, V. Oreshkin, I. Smirnov, V. Sulimov, L. Uvarov, S. Vavilov, A. Vorobyev

Institute for Nuclear Research, Moscow, Russia

Yu. Andreev, A. Dermenev, S. Gninenko, N. Golubev, A. Karneyeu, M. Kirsanov, N. Krasnikov, A. Pashenkov, D. Tlisov, A. Toropin

Institute for Theoretical and Experimental Physics, Moscow, Russia

V. Epshteyn, V. Gavrillov, N. Lychkovskaya, V. Popov, I. Pozdnyakov, G. Safronov, A. Spiridonov, E. Vlasov, A. Zhokin

National Research Nuclear University 'Moscow Engineering Physics Institute' (MEPhI), Moscow, Russia

A. Bylinkin

P.N. Lebedev Physical Institute, Moscow, Russia

V. Andreev, M. Azarkin³⁶, I. Dremin³⁶, M. Kirakosyan, A. Leonidov³⁶, G. Mesyats, S.V. Rusakov, A. Vinogradov

Skobeltsyn Institute of Nuclear Physics, Lomonosov Moscow State University, Moscow, Russia

A. Baskakov, A. Belyaev, E. Boos, M. Dubinin³⁷, L. Dudko, A. Ershov, A. Gribushin, V. Klyukhin, O. Kodolova, I. Lokhtin, I. Myagkov, S. Obraztsov, S. Petrushanko, V. Savrin, A. Snigirev

State Research Center of Russian Federation, Institute for High Energy Physics, Protvino, Russia

I. Azhgirey, I. Bayshev, S. Bitioukov, V. Kachanov, A. Kalinin, D. Konstantinov, V. Krychkin, V. Petrov, R. Ryutin, A. Sobol, L. Tourtchanovitch, S. Troshin, N. Tyurin, A. Uzunian, A. Volkov

University of Belgrade, Faculty of Physics and Vinca Institute of Nuclear Sciences, Belgrade, Serbia

P. Adzic³⁸, M. Ekmedzic, J. Milosevic, V. Rekovic

Centro de Investigaciones Energéticas Medioambientales y Tecnológicas (CIEMAT), Madrid, Spain

J. Alcaraz Maestre, E. Calvo, M. Cerrada, M. Chamizo Llatas, N. Colino, B. De La Cruz, A. Delgado Peris, D. Domínguez Vázquez, A. Escalante Del Valle, C. Fernandez Bedoya, J.P. Fernández Ramos, J. Flix, M.C. Fouz, P. Garcia-Abia, O. Gonzalez Lopez, S. Goy Lopez, J.M. Hernandez, M.I. Josa, E. Navarro De Martino, A. Pérez-Calero Yzquierdo, J. Puerta Pelayo, A. Quintario Olmeda, I. Redondo, L. Romero, M.S. Soares

Universidad Autónoma de Madrid, Madrid, Spain

C. Albajar, J.F. de Trocóniz, M. Missiroli, D. Moran

Universidad de Oviedo, Oviedo, Spain

H. Brun, J. Cuevas, J. Fernandez Menendez, S. Folgueras, I. Gonzalez Caballero, E. Palencia Cortezon, J.M. Vizan Garcia

Instituto de Física de Cantabria (IFCA), CSIC-Universidad de Cantabria, Santander, Spain

J.A. Brochero Cifuentes, I.J. Cabrillo, A. Calderon, J.R. Castiñeiras De Saa, J. Duarte Campderros, M. Fernandez, G. Gomez, A. Graziano, A. Lopez Virto, J. Marco, R. Marco, C. Martinez Rivero, F. Matorras, F.J. Munoz Sanchez, J. Piedra Gomez, T. Rodrigo, A.Y. Rodríguez-Marrero, A. Ruiz-Jimeno, L. Scodellaro, I. Vila, R. Vilar Cortabitarte

CERN, European Organization for Nuclear Research, Geneva, Switzerland

D. Abbaneo, E. Auffray, G. Auzinger, M. Bachtis, P. Baillon, A.H. Ball, D. Barney, A. Benaglia, J. Bendavid, L. Benhabib, J.F. Benitez, G.M. Berruti, G. Bianchi, P. Bloch, A. Bocci, A. Bonato, C. Botta, H. Breuker, T. Camporesi, G. Cerminara, S. Colafranceschi³⁹, M. D'Alfonso, D. d'Enterria, A. Dabrowski, V. Daponte, A. David, M. De Gruttola, F. De Guio, A. De Roeck, S. De Visscher, E. Di Marco, M. Dobson, M. Dordevic, T. du Pree, N. Dupont-Sagorin, A. Elliott-Peisert, J. Eugster, G. Franzoni, W. Funk, D. Gigi, K. Gill, D. Giordano, M. Girone, F. Glege, R. Guida, S. Gundacker, M. Guthoff, J. Hammer, M. Hansen, P. Harris, J. Hegeman, V. Innocente, P. Janot, H. Kirschenmann, M.J. Kortelainen, K. Kousouris, K. Krajczar, P. Lecoq, C. Lourenço, M.T. Lucchini, N. Magini, L. Malgeri, M. Mannelli, J. Marrouche, A. Martelli, L. Masetti, F. Meijers, S. Mersi, E. Meschi, F. Moortgat, S. Morovic, M. Mulders, M.V. Nemallapudi, H. Neugebauer, S. Orfanelli⁴⁰, L. Orsini, L. Pape, E. Perez, A. Petrilli, G. Petrucciani, A. Pfeiffer, D. Piparo, A. Racz, G. Rolandi⁴¹, M. Rovere, M. Ruan, H. Sakulin, C. Schäfer, C. Schwick, A. Sharma, P. Silva, M. Simon, P. Sphicas⁴², D. Spiga, J. Steggemann, B. Stieger, M. Stoye, Y. Takahashi, D. Treille, A. Tsiros, G.I. Veres²⁰, N. Wardle, H.K. Wöhri, A. Zagozdinska⁴³, W.D. Zeuner

Paul Scherrer Institut, Villigen, Switzerland

W. Bertl, K. Deiters, W. Erdmann, R. Horisberger, Q. Ingram, H.C. Kaestli, D. Kotlinski, U. Langenegger, T. Rohe

Institute for Particle Physics, ETH Zurich, Zurich, Switzerland

F. Bachmair, L. Bäni, L. Bianchini, M.A. Buchmann, B. Casal, G. Dissertori, M. Dittmar, M. Donegà, M. Dünser, P. Eller, C. Grab, C. Heidegger, D. Hits, J. Hoss, G. Kasieczka, W. Lustermann, B. Mangano, A.C. Marini, M. Marionneau, P. Martinez Ruiz del Arbol, M. Masciovecchio, D. Meister, N. Mohr, P. Musella, F. Nessi-Tedaldi, F. Pandolfi, J. Pata, F. Pauss, L. Perrozzi, M. Peruzzi, M. Quittnat, M. Rossini, A. Starodumov⁴⁴, M. Takahashi, V.R. Tavolaro, K. Theofilatos, R. Wallny, H.A. Weber

Universität Zürich, Zurich, Switzerland

T.K. Aarrestad, C. Amsler⁴⁵, M.F. Canelli, V. Chiochia, A. De Cosa, C. Galloni, A. Hinzmann, T. Hreus, B. Kilminster, C. Lange, J. Ngadiuba, D. Pinna, P. Robmann, F.J. Ronga, D. Salerno, S. Taroni, Y. Yang

National Central University, Chung-Li, Taiwan

M. Cardaci, K.H. Chen, T.H. Doan, C. Ferro, M. Konyushikhin, C.M. Kuo, W. Lin, Y.J. Lu, R. Volpe, S.S. Yu

National Taiwan University (NTU), Taipei, Taiwan

P. Chang, Y.H. Chang, Y.W. Chang, Y. Chao, K.F. Chen, P.H. Chen, C. Dietz, F. Fiori, U. Grundler, W.-S. Hou, Y. Hsiung, Y.F. Liu, R.-S. Lu, M. Miñano Moya, E. Petrakou, J.f. Tsai, Y.M. Tzeng, R. Wilken

Chulalongkorn University, Faculty of Science, Department of Physics, Bangkok, Thailand

B. Asavapibhop, K. Kovitanggoon, G. Singh, N. Srimanobhas, N. Suwonjandee

Cukurova University, Adana, Turkey

A. Adiguzel, M.N. Bakirci⁴⁶, C. Dozen, I. Dumanoglu, E. Eskut, S. Girgis, G. Gokbulut, Y. Guler, E. Gurpinar, I. Hos, E.E. Kangal⁴⁷, G. Onengut⁴⁸, K. Ozdemir⁴⁹, A. Polatoz, D. Sunar Cerci⁵⁰, M. Vergili, C. Zorbilmez

Middle East Technical University, Physics Department, Ankara, Turkey

I.V. Akin, B. Bilin, S. Bilmis, B. Isildak⁵¹, G. Karapinar⁵², U.E. Surat, M. Yalvac, M. Zeyrek

Bogazici University, Istanbul, Turkey

E.A. Albayrak⁵³, E. Gülmez, M. Kaya⁵⁴, O. Kaya⁵⁵, T. Yetkin⁵⁶

Istanbul Technical University, Istanbul, Turkey

K. Cankocak, F.I. Vardarli

Institute for Scintillation Materials of National Academy of Science of Ukraine, Kharkov, Ukraine

B. Grynyov

National Scientific Center, Kharkov Institute of Physics and Technology, Kharkov, Ukraine

L. Levchuk, P. Sorokin

University of Bristol, Bristol, United Kingdom

R. Aggleton, F. Ball, L. Beck, J.J. Brooke, E. Clement, D. Cussans, H. Flacher, J. Goldstein, M. Grimes, G.P. Heath, H.F. Heath, J. Jacob, L. Kreczko, C. Lucas, Z. Meng, D.M. Newbold⁵⁷, S. Paramesvaran, A. Poll, T. Sakuma, S. Seif El Nasr-storey, S. Senkin, D. Smith, V.J. Smith

Rutherford Appleton Laboratory, Didcot, United Kingdom

K.W. Bell, A. Belyaev⁵⁸, C. Brew, R.M. Brown, D.J.A. Cockerill, J.A. Coughlan, K. Harder, S. Harper, E. Olaiya, D. Petyt, C.H. Shepherd-Themistocleous, A. Thea, I.R. Tomalin, T. Williams, W.J. Womersley, S.D. Worm

Imperial College, London, United Kingdom

M. Baber, R. Bainbridge, O. Buchmuller, A. Bundock, D. Burton, S. Casasso, M. Citron, D. Colling, L. Corpe, N. Cripps, P. Dauncey, G. Davies, A. De Wit, M. Della Negra, P. Dunne, A. Elwood, W. Ferguson, J. Fulcher, D. Futyan, G. Hall, G. Iles, G. Karapostoli, M. Kenzie, R. Lane, R. Lucas⁵⁷, L. Lyons, A.-M. Magnan, S. Malik, J. Nash, A. Nikitenko⁴⁴, J. Pela, M. Pesaresi, K. Petridis, D.M. Raymond, A. Richards, A. Rose, C. Seez, P. Sharp[†], A. Tapper, K. Uchida, M. Vazquez Acosta⁵⁹, T. Virdee, S.C. Zenz

Brunel University, Uxbridge, United Kingdom

J.E. Cole, P.R. Hobson, A. Khan, P. Kyberd, D. Leggat, D. Leslie, I.D. Reid, P. Symonds, L. Teodorescu, M. Turner

Baylor University, Waco, USA

A. Borzou, J. Dittmann, K. Hatakeyama, A. Kasmi, H. Liu, N. Pastika

The University of Alabama, Tuscaloosa, USA

O. Charaf, S.I. Cooper, C. Henderson, P. Rumerio

Boston University, Boston, USA

A. Avetisyan, T. Bose, C. Fantasia, D. Gastler, P. Lawson, D. Rankin, C. Richardson, J. Rohlf, J. St. John, L. Sulak, D. Zou

Brown University, Providence, USA

J. Alimena, E. Berry, S. Bhattacharya, D. Cutts, Z. Demiragli, N. Dhingra, A. Ferapontov, A. Garabedian, U. Heintz, E. Laird, G. Landsberg, Z. Mao, M. Narain, S. Sagir, T. Sinthuprasith

University of California, Davis, Davis, USA

R. Breedon, G. Breto, M. Calderon De La Barca Sanchez, S. Chauhan, M. Chertok, J. Conway, R. Conway, P.T. Cox, R. Erbacher, M. Gardner, W. Ko, R. Lander, M. Mulhearn, D. Pellett, J. Pilot, F. Ricci-Tam, S. Shalhout, J. Smith, M. Squires, D. Stolp, M. Tripathi, S. Wilbur, R. Yohay

University of California, Los Angeles, USA

R. Cousins, P. Everaerts, C. Farrell, J. Hauser, M. Ignatenko, G. Rakness, D. Saltzberg, E. Takasugi, V. Valuev, M. Weber

University of California, Riverside, Riverside, USA

K. Burt, R. Clare, J. Ellison, J.W. Gary, G. Hanson, J. Heilman, M. Ivova Rikova, P. Jandir, E. Kennedy, F. Lacroix, O.R. Long, A. Luthra, M. Malberti, M. Olmedo Negrete, A. Shrinivas, S. Sumowidagdo, H. Wei, S. Wimpenny

University of California, San Diego, La Jolla, USA

J.G. Branson, G.B. Cerati, S. Cittolin, R.T. D'Agnolo, A. Holzner, R. Kelley, D. Klein, J. Letts, I. Macneill, D. Olivito, S. Padhi, M. Pieri, M. Sani, V. Sharma, S. Simon, M. Tadel, Y. Tu, A. Vartak, S. Wasserbaech⁶⁰, C. Welke, F. Würthwein, A. Yagil, G. Zevi Della Porta

University of California, Santa Barbara, Santa Barbara, USA

D. Barge, J. Bradmiller-Feld, C. Campagnari, A. Dishaw, V. Dutta, K. Flowers, M. Franco Sevilla, P. Geffert, C. George, F. Golf, L. Gouskos, J. Gran, J. Incandela, C. Justus, N. Mccoll, S.D. Mullin, J. Richman, D. Stuart, I. Suarez, W. To, C. West, J. Yoo

California Institute of Technology, Pasadena, USA

D. Anderson, A. Apresyan, A. Bornheim, J. Bunn, Y. Chen, J. Duarte, A. Mott, H.B. Newman, C. Pena, M. Pierini, M. Spiropulu, J.R. Vlimant, S. Xie, R.Y. Zhu

Carnegie Mellon University, Pittsburgh, USA

V. Azzolini, A. Calamba, B. Carlson, T. Ferguson, Y. Iiyama, M. Paulini, J. Russ, M. Sun, H. Vogel, I. Vorobiev

University of Colorado at Boulder, Boulder, USA

J.P. Cumalat, W.T. Ford, A. Gaz, F. Jensen, A. Johnson, M. Krohn, T. Mulholland, U. Nauenberg, J.G. Smith, K. Stenson, S.R. Wagner

Cornell University, Ithaca, USA

J. Alexander, A. Chatterjee, J. Chaves, J. Chu, S. Dittmer, N. Eggert, N. Mirman, G. Nicolas Kaufman, J.R. Patterson, A. Rinkevicius, A. Ryd, L. Skinnari, L. Soffi, W. Sun, S.M. Tan, W.D. Teo, J. Thom, J. Thompson, J. Tucker, Y. Weng, P. Wittich

Fermi National Accelerator Laboratory, Batavia, USA

S. Abdullin, M. Albrow, J. Anderson, G. Apollinari, L.A.T. Bauerdick, A. Beretvas, J. Berryhill, P.C. Bhat, G. Bolla, K. Burkett, J.N. Butler, H.W.K. Cheung, F. Chlebana, S. Cihangir, V.D. Elvira, I. Fisk, J. Freeman, E. Gottschalk, L. Gray, D. Green, S. Grünendahl, O. Gutsche, J. Hanlon, D. Hare, R.M. Harris, J. Hirschauer, B. Hooberman, Z. Hu, S. Jindariani, M. Johnson, U. Joshi, A.W. Jung, B. Klima, B. Kreis, S. Kwan[†], S. Lammel, J. Linacre, D. Lincoln, R. Lipton, T. Liu, R. Lopes De Sá, J. Lykken, K. Maeshima, J.M. Marraffino, V.I. Martinez Outschoorn, S. Maruyama, D. Mason, P. McBride, P. Merkel, K. Mishra, S. Mrenna, S. Nahn, C. Newman-Holmes, V. O'Dell, O. Prokofyev, E. Sexton-Kennedy, A. Soha, W.J. Spalding, L. Spiegel,

L. Taylor, S. Tkaczyk, N.V. Tran, L. Uplegger, E.W. Vaandering, C. Vernieri, M. Verzocchi, R. Vidal, A. Whitbeck, F. Yang, H. Yin

University of Florida, Gainesville, USA

D. Acosta, P. Avery, P. Bortignon, D. Bourilkov, A. Carnes, M. Carver, D. Curry, S. Das, G.P. Di Giovanni, R.D. Field, M. Fisher, I.K. Furic, J. Hugon, J. Konigsberg, A. Korytov, J.F. Low, P. Ma, K. Matchev, H. Mei, P. Milenovic⁶¹, G. Mitselmakher, L. Muniz, D. Rank, L. Shchutska, M. Snowball, D. Sperka, S.J. Wang, J. Yelton

Florida International University, Miami, USA

S. Hewamanage, S. Linn, P. Markowitz, G. Martinez, J.L. Rodriguez

Florida State University, Tallahassee, USA

A. Ackert, J.R. Adams, T. Adams, A. Askew, J. Bochenek, B. Diamond, J. Haas, S. Hagopian, V. Hagopian, K.F. Johnson, A. Khatiwada, H. Prosper, V. Veeraraghavan, M. Weinberg

Florida Institute of Technology, Melbourne, USA

V. Bhopatkar, M. Hohlmann, H. Kalakhety, D. Mareskas-palcek, T. Roy, F. Yumiceva

University of Illinois at Chicago (UIC), Chicago, USA

M.R. Adams, L. Apanasevich, D. Berry, R.R. Betts, I. Bucinskaite, R. Cavanaugh, O. Evdokimov, L. Gauthier, C.E. Gerber, D.J. Hofman, P. Kurt, C. O'Brien, I.D. Sandoval Gonzalez, C. Silkworth, P. Turner, N. Varelas, Z. Wu, M. Zakaria

The University of Iowa, Iowa City, USA

B. Bilki⁶², W. Clarida, K. Dilsiz, S. Durgut, R.P. Gandrajula, M. Haytmyradov, V. Khristenko, J.-P. Merlo, H. Mermerkaya⁶³, A. Mestvirishvili, A. Moeller, J. Nachtman, H. Ogul, Y. Onel, F. Ozok⁵³, A. Penzo, S. Sen⁶⁴, C. Snyder, P. Tan, E. Tiras, J. Wetzel, K. Yi

Johns Hopkins University, Baltimore, USA

I. Anderson, B.A. Barnett, B. Blumenfeld, D. Fehling, L. Feng, A.V. Gritsan, P. Maksimovic, C. Martin, K. Nash, M. Osherson, M. Swartz, M. Xiao, Y. Xin

The University of Kansas, Lawrence, USA

P. Baringer, A. Bean, G. Benelli, C. Bruner, J. Gray, R.P. Kenny III, D. Majumder, M. Malek, M. Murray, D. Noonan, S. Sanders, R. Stringer, Q. Wang, J.S. Wood

Kansas State University, Manhattan, USA

I. Chakaberia, A. Ivanov, K. Kaadze, S. Khalil, M. Makouski, Y. Maravin, L.K. Saini, N. Skhirtladze, I. Svintradze, S. Toda

Lawrence Livermore National Laboratory, Livermore, USA

D. Lange, F. Rebassoo, D. Wright

University of Maryland, College Park, USA

C. Anelli, A. Baden, O. Baron, A. Belloni, B. Calvert, S.C. Eno, C. Ferraioli, J.A. Gomez, N.J. Hadley, S. Jabeen, R.G. Kellogg, T. Kolberg, J. Kunkle, Y. Lu, A.C. Mignerey, K. Pedro, Y.H. Shin, A. Skuja, M.B. Tonjes, S.C. Tonwar

Massachusetts Institute of Technology, Cambridge, USA

A. Apyan, R. Barbieri, A. Baty, K. Bierwagen, S. Brandt, W. Busza, I.A. Cali, L. Di Matteo, G. Gomez Ceballos, M. Goncharov, D. Gulhan, G.M. Innocenti, M. Klute, D. Kovalskyi, Y.S. Lai, Y.-J. Lee, A. Levin, P.D. Luckey, C. McGinn, X. Niu, C. Paus, D. Ralph, C. Roland, G. Roland, G.S.F. Stephens, K. Sumorok, M. Varma, D. Velicanu, J. Veverka, J. Wang, T.W. Wang, B. Wyslouch, M. Yang, V. Zhukova

University of Minnesota, Minneapolis, USA

B. Dahmes, A. Finkel, A. Gude, P. Hansen, S. Kalafut, S.C. Kao, K. Klapoetke, Y. Kubota, Z. Lesko, J. Mans, S. Nourbakhsh, N. Ruckstuhl, R. Rusack, N. Tambe, J. Turkewitz

University of Mississippi, Oxford, USA

J.G. Acosta, S. Oliveros

University of Nebraska-Lincoln, Lincoln, USA

E. Avdeeva, K. Bloom, S. Bose, D.R. Claes, A. Dominguez, C. Fangmeier, R. Gonzalez Suarez, R. Kamalieddin, J. Keller, D. Knowlton, I. Kravchenko, J. Lazo-Flores, F. Meier, J. Monroy, F. Ratnikov, J.E. Siado, G.R. Snow

State University of New York at Buffalo, Buffalo, USA

M. Alyari, J. Dolen, J. George, A. Godshalk, I. Iashvili, J. Kaisen, A. Kharchilava, A. Kumar, S. Rappoccio

Northeastern University, Boston, USA

G. Alverson, E. Barberis, D. Baumgartel, M. Chasco, A. Hortiangtham, A. Massironi, D.M. Morse, D. Nash, T. Orimoto, R. Teixeira De Lima, D. Trocino, R.-J. Wang, D. Wood, J. Zhang

Northwestern University, Evanston, USA

K.A. Hahn, A. Kubik, N. Mucia, N. Odell, B. Pollack, A. Pozdnyakov, M. Schmitt, S. Stoynev, K. Sung, M. Trovato, M. Velasco, S. Won

University of Notre Dame, Notre Dame, USA

A. Brinkerhoff, N. Dev, M. Hildreth, C. Jessop, D.J. Karmgard, N. Kellams, K. Lannon, S. Lynch, N. Marinelli, F. Meng, C. Mueller, Y. Musienko³³, T. Pearson, M. Planer, R. Ruchti, G. Smith, N. Valls, M. Wayne, M. Wolf, A. Woodard

The Ohio State University, Columbus, USA

L. Antonelli, J. Brinson, B. Bylsma, L.S. Durkin, S. Flowers, A. Hart, C. Hill, R. Hughes, K. Kotov, T.Y. Ling, B. Liu, W. Luo, D. Puigh, M. Rodenburg, B.L. Winer, H.W. Wulsin

Princeton University, Princeton, USA

O. Driga, P. Elmer, J. Hardenbrook, P. Hebda, S.A. Koay, P. Lujan, D. Marlow, T. Medvedeva, M. Mooney, J. Olsen, C. Palmer, P. Piroué, X. Quan, H. Saka, D. Stickland, C. Tully, J.S. Werner, A. Zuranski

Purdue University, West Lafayette, USA

V.E. Barnes, D. Benedetti, D. Bortoletto, L. Gutay, M.K. Jha, M. Jones, K. Jung, M. Kress, N. Leonardo, D.H. Miller, N. Neumeister, F. Primavera, B.C. Radburn-Smith, X. Shi, I. Shipsey, D. Silvers, J. Sun, A. Svyatkovskiy, F. Wang, W. Xie, L. Xu, J. Zablocki

Purdue University Calumet, Hammond, USA

N. Parashar, J. Stupak

Rice University, Houston, USA

A. Adair, B. Akgun, Z. Chen, K.M. Ecklund, F.J.M. Geurts, M. Guilbaud, W. Li, B. Michlin, M. Northup, B.P. Padley, R. Redjimi, J. Roberts, J. Rorie, Z. Tu, J. Zabel

University of Rochester, Rochester, USA

B. Betchart, A. Bodek, P. de Barbaro, R. Demina, Y. Eshaq, T. Ferbel, M. Galanti, A. Garcia-Bellido, P. Goldenzweig, J. Han, A. Harel, O. Hindrichs, A. Khukhunaishvili, G. Petrillo, M. Verzetti

The Rockefeller University, New York, USA

L. Demortier

Rutgers, The State University of New Jersey, Piscataway, USA

S. Arora, A. Barker, J.P. Chou, C. Contreras-Campana, E. Contreras-Campana, D. Duggan, D. Ferencek, Y. Gershtein, R. Gray, E. Halkiadakis, D. Hidas, E. Hughes, S. Kaplan, R. Kunnawalkam Elayavalli, A. Lath, S. Panwalkar, M. Park, S. Salur, S. Schnetzer, D. Sheffield, S. Somalwar, R. Stone, S. Thomas, P. Thomassen, M. Walker

University of Tennessee, Knoxville, USA

M. Foerster, G. Riley, K. Rose, S. Spanier, A. York

Texas A&M University, College Station, USA

O. Bouhali⁶⁵, A. Castaneda Hernandez, M. Dalchenko, M. De Mattia, A. Delgado, S. Dildick, R. Eusebi, W. Flanagan, J. Gilmore, T. Kamon⁶⁶, V. Krutelyov, R. Montalvo, R. Mueller, I. Osipenkov, Y. Pakhotin, R. Patel, A. Perloff, J. Roe, A. Rose, A. Safonov, A. Tatarinov, K.A. Ulmer²

Texas Tech University, Lubbock, USA

N. Akchurin, C. Cowden, J. Damgov, C. Dragoiu, P.R. Duderod, J. Faulkner, S. Kunori, K. Lamichhane, S.W. Lee, T. Libeiro, S. Undleeb, I. Volobouev

Vanderbilt University, Nashville, USA

E. Appelt, A.G. Delannoy, S. Greene, A. Gurrola, R. Janjam, W. Johns, C. Maguire, Y. Mao, A. Melo, P. Sheldon, B. Snook, S. Tuo, J. Velkovska, Q. Xu

University of Virginia, Charlottesville, USA

M.W. Arenton, S. Boutle, B. Cox, B. Francis, J. Goodell, R. Hirosky, A. Ledovskoy, H. Li, C. Lin, C. Neu, E. Wolfe, J. Wood, F. Xia

Wayne State University, Detroit, USA

C. Clarke, R. Harr, P.E. Karchin, C. Kottachchi Kankanamge Don, P. Lamichhane, J. Sturdy

University of Wisconsin, Madison, USA

D.A. Belknap, D. Carlsmith, M. Cepeda, A. Christian, S. Dasu, L. Dodd, S. Duric, E. Friis, B. Gomber, M. Grothe, R. Hall-Wilton, M. Herndon, A. Hervé, P. Klabbers, A. Lanaro, A. Levine, K. Long, R. Loveless, A. Mohapatra, I. Ojalvo, T. Perry, G.A. Pierro, G. Polese, I. Ross, T. Ruggles, T. Sarangi, A. Savin, N. Smith, W.H. Smith, D. Taylor, N. Woods

†: Deceased

1: Also at Vienna University of Technology, Vienna, Austria

2: Also at CERN, European Organization for Nuclear Research, Geneva, Switzerland

3: Also at State Key Laboratory of Nuclear Physics and Technology, Peking University, Beijing, China

4: Also at Institut Pluridisciplinaire Hubert Curien, Université de Strasbourg, Université de Haute Alsace Mulhouse, CNRS/IN2P3, Strasbourg, France

5: Also at National Institute of Chemical Physics and Biophysics, Tallinn, Estonia

6: Also at Skobeltsyn Institute of Nuclear Physics, Lomonosov Moscow State University, Moscow, Russia

7: Also at Universidade Estadual de Campinas, Campinas, Brazil

8: Also at Centre National de la Recherche Scientifique (CNRS) - IN2P3, Paris, France

9: Also at Laboratoire Leprince-Ringuet, Ecole Polytechnique, IN2P3-CNRS, Palaiseau, France

10: Also at Joint Institute for Nuclear Research, Dubna, Russia

11: Also at Ain Shams University, Cairo, Egypt

- 12: Now at British University in Egypt, Cairo, Egypt
- 13: Now at Helwan University, Cairo, Egypt
- 14: Also at Suez University, Suez, Egypt
- 15: Also at Cairo University, Cairo, Egypt
- 16: Now at Fayoum University, El-Fayoum, Egypt
- 17: Also at Université de Haute Alsace, Mulhouse, France
- 18: Also at Brandenburg University of Technology, Cottbus, Germany
- 19: Also at Institute of Nuclear Research ATOMKI, Debrecen, Hungary
- 20: Also at Eötvös Loránd University, Budapest, Hungary
- 21: Also at University of Debrecen, Debrecen, Hungary
- 22: Also at Wigner Research Centre for Physics, Budapest, Hungary
- 23: Also at University of Visva-Bharati, Santiniketan, India
- 24: Now at King Abdulaziz University, Jeddah, Saudi Arabia
- 25: Also at University of Ruhuna, Matara, Sri Lanka
- 26: Also at Isfahan University of Technology, Isfahan, Iran
- 27: Also at University of Tehran, Department of Engineering Science, Tehran, Iran
- 28: Also at Plasma Physics Research Center, Science and Research Branch, Islamic Azad University, Tehran, Iran
- 29: Also at Università degli Studi di Siena, Siena, Italy
- 30: Also at Purdue University, West Lafayette, USA
- 31: Also at International Islamic University of Malaysia, Kuala Lumpur, Malaysia
- 32: Also at CONSEJO NACIONAL DE CIENCIA Y TECNOLOGIA, MEXICO, Mexico
- 33: Also at Institute for Nuclear Research, Moscow, Russia
- 34: Also at Institute of High Energy Physics and Informatization, Tbilisi State University, Tbilisi, Georgia
- 35: Also at St. Petersburg State Polytechnical University, St. Petersburg, Russia
- 36: Also at National Research Nuclear University 'Moscow Engineering Physics Institute' (MEPhI), Moscow, Russia
- 37: Also at California Institute of Technology, Pasadena, USA
- 38: Also at Faculty of Physics, University of Belgrade, Belgrade, Serbia
- 39: Also at Facoltà Ingegneria, Università di Roma, Roma, Italy
- 40: Also at National Technical University of Athens, Athens, Greece
- 41: Also at Scuola Normale e Sezione dell'INFN, Pisa, Italy
- 42: Also at University of Athens, Athens, Greece
- 43: Also at Warsaw University of Technology, Institute of Electronic Systems, Warsaw, Poland
- 44: Also at Institute for Theoretical and Experimental Physics, Moscow, Russia
- 45: Also at Albert Einstein Center for Fundamental Physics, Bern, Switzerland
- 46: Also at Gaziosmanpasa University, Tokat, Turkey
- 47: Also at Mersin University, Mersin, Turkey
- 48: Also at Cag University, Mersin, Turkey
- 49: Also at Piri Reis University, Istanbul, Turkey
- 50: Also at Adiyaman University, Adiyaman, Turkey
- 51: Also at Ozyegin University, Istanbul, Turkey
- 52: Also at Izmir Institute of Technology, Izmir, Turkey
- 53: Also at Mimar Sinan University, Istanbul, Istanbul, Turkey
- 54: Also at Marmara University, Istanbul, Turkey
- 55: Also at Kafkas University, Kars, Turkey
- 56: Also at Yildiz Technical University, Istanbul, Turkey
- 57: Also at Rutherford Appleton Laboratory, Didcot, United Kingdom

58: Also at School of Physics and Astronomy, University of Southampton, Southampton, United Kingdom

59: Also at Instituto de Astrofísica de Canarias, La Laguna, Spain

60: Also at Utah Valley University, Orem, USA

61: Also at University of Belgrade, Faculty of Physics and Vinca Institute of Nuclear Sciences, Belgrade, Serbia

62: Also at Argonne National Laboratory, Argonne, USA

63: Also at Erzincan University, Erzincan, Turkey

64: Also at Hacettepe University, Ankara, Turkey

65: Also at Texas A&M University at Qatar, Doha, Qatar

66: Also at Kyungpook National University, Daegu, Korea